Journal of Energy Storage 22 (2019) 355–372

Contents lists available at ScienceDirect

Journal of Energy Storage

journal homepage: www.elsevier.com/locate/est

Computational investigation of bounded domain with different orientations using CPCM

Santosh Chavan, Veershetty Gumtapure, D. Arumuga Perumal*

Department of Mechanical Engineering, National Institute of Technology Karnataka, Surathkal, Mangalore 575025, India

ARTICLE INFO

Keywords:
Composite phase change material (CPCM)
Heat transfer enhancement
Nanoparticles
Paraffin wax
Bounded domain

ABSTRACT

The present work deals with the composite phase change material (CPCM) of 98% paraffin wax and 2% copper nanoparticle, filled into the bounded domain. Effects of orientation (45°, 90°, 135° and 180°) with different wall heating conditions (base, left and top wall) are analyzed numerically to understand the flow patterns and interface morphology developed during melting/solidification processes. The melting/solidification mechanism exhibited non-uniform flow patterns and irregular morphology which are dependent on geometrical orientations and different wall heating conditions. The results revealed that the bounded domain with different orientations have significant effect on natural convection current formation. As the orientation changes, the heat transfer rate gets influenced significantly and convection currents amplifies. Top wall heating arrangement of 180° orientation shows competence in achieving better thermal performance.

1. Introduction

Presently, energy storage is a worldwide concern due to the intermittency of solar thermal energy sources, to associate the mismatch between source and requirement use of phase change material (PCM) is an attractive alternative. The intermittency of available thermal energy thrusts toward thermal energy storage techniques, advancement of technology is obligatory due to the incompetence of present systems. To confront the problem design customization and selection of the best material is imperative. PCM stores large amounts of heat energy with minimum volume requirement at constant temperature [1]. A large number of PCMs are commercially available depending on energy storage capacity and the working temperature range.

A considerable amount of thermal energy is available at a lower temperature through various operations, which is generally drained to sink (like exhaust gases from thermal power plants and various process industries, solar energy and large electronic equipment). This energy can be stored and used for secondary applications like water preheating in power plants and textile industries for dying [2]. It is known that, PCMs are extensively preferred because of its higher thermal storage capacity. The volume requirement is relatively low but its low thermal conductivity makes it unattractive toward thermal energy storage (TES) systems.

Numerous researchers are working to enhance the thermal conductivity of PCMs to compensate for thermal performance. However, the heat transfer rate and thermal conductivity can be improved by blending nanoparticles. Various thermal analysis is carried out and the thermal performance is evaluated by using flow and heat transfer characteristics like streamline patterns, morphological changes in melting zone, the progress of the melting front and evolution of melting fraction [3]. To eliminate and improve undesired properties of the storage material various methods and technologies are adopted, such as blending with suitable nanoparticles, geometrical modifications and encapsulation techniques. Blending of highly conductive materials like carbon-based nanoparticles such as graphene, carbon nanotubes (CNT), fullerene, etc., in the PCM improves the thermal storage performance. Copper and Al_2O_3 nanoparticles also demonstrated the enhancement of thermal conductivity in paraffin wax [4].

Melting and solidification time depends on geometrical orientations, thermal parameters and thermophysical properties of PCMs. In most of the experimental and numerical investigations geometrical model used is square or bounded domain due to their wide range of engineering applications. The interface structures are used to understand the streamline patterns of the energy transport mechanism and the streamline patterns are dependent on the orientation of the geometry [5]. The orientation of domain affects significantly on the melting process, as the angle of orientation increased non-uniformity is seen in the melting/solidification process [6]. A composite phase change material (CPCM) or polymer mixture is a new class of materials, in which at least two polymers are blended together to create a new

* Corresponding author.
E-mail address: perumal@nitk.edu.in (D. Arumuga Perumal).

https://doi.org/10.1016/j.est.2019.02.018
Received 17 November 2018; Received in revised form 15 February 2019; Accepted 15 February 2019

material with different physical properties in order to enhance thermophysical characteristics [7,8].

Recent investigations are focused on composites of wax and the supporting matrix of low-density polyethylene (LDPE) for effective thermal energy storage applications. Because this type of composites materials can be used for latent heat storage systems without encapsulation, this method provides some advantages over traditional methods. The CPCMs offers higher thermal storage capacity even at a lower temperature range in the building applications, storage components can give extensive heat transfer area and they can be effortlessly brought and introduced with existing facilities. To improve the thermophysical properties of LDPE nano-silica nanoparticles are uniformly dispersed which reduced the polarity of the silica surface and improved the thermal performance by improving the thermal stability of the polymer matrix [9,10].

For low-temperature range of 20–50 °C, the thermal energy storage compatibility is analyzed using composite phase change material (CPCM) of linear low-density polyethylene (LLDPE), paraffin wax and expanded graphite (EG). The composite results reduction in sensible heat with EG. Carbon-based nanoparticle loading also exhibited similar response and melting/solidification time reduced by enhancing the thermal conductivity [11–14]. The crystallization behavior of LLDPE and the degree of supercooling during melting/solidification process shows reversed patterns of unimodal and bimodal LLDPE crystallization rates with average supercooling. The impact of the high molar mass constituent present in the bimodal material gradually becomes dominant as super-cooling increases [15]. The super-cooling phenomenon is extremely common in the phase change materials during solid–liquid phase transition [16].

To study the structural stability of the PCMs various experiments are carried out at optimum molding pressure and time. To achieve higher thermal conductivity and overcome the poor shape stability Al/Al_2O_3 form stable CPCM are developed and used for high-temperature range thermal energy storage application as a reliable and efficient material [17]. The shape stability greatly affects when the PCMs are operated above the phase transition temperature for longer period of time. To maintain the effectiveness of working material either it is encapsulated or nucleating and thickening agent materials are used as additives. High-density polyethylene (HDPE) is also used to study the thermal stability and leakage, the results demonstrated reduction in the leakage percentage with different additive concentrations. Pure HDPE has shown maximum leakage and 5% loading of additive material shown least leakage with better thermal stability [18].

2. Problem description

The numerical studies of melting/solidification characteristics of CPCM filled into the bounded domain with different geometrical orientations are considered. Fig. 1 shows the Geometrical representation of 2-D model with different orientations.

A bounded domain is filled with CPCM (98% paraffin mixed with 2% nanoparticles) and used as a thermal storage medium (TSM). To achieve the realistic results similar to the practical situation some assumptions are made, which are listed below.

(i) Working fluid in the melting phase is Newtonian fluid and the flow is incompressible;
(ii) The flow in the melting phase is laminar with negligible viscous dissipation rate;
(iii) The thermophysical properties of CPCM are purely temperature dependent;
(iv) The change of volume during phase transition is negligible and the CPCM solid is in contact with the cold wall at all times.

The numerical study is carried out for four different orientations of the geometrical model for the same geometry by changing in clockwise direction with the increment of 45°: (a) 45° orientation, (b) 90° (deep) orientation, (c) 135° orientation and (d) 180° (shallow) orientation.

Table 1
Thermophysical properties of copper nanoparticles and paraffin wax [19].

Sl.no	Properties	Nano additives	Base phase change material
		Copper	Paraffin wax
1	Density (kg/m^3)	8954	$\frac{750}{0.001(T-319.15)+1}$
2	Specific heat (J/kg K)	383	2890
3	Thermal conductivity (W/m K)	400	0.21 if $T < T_{solidus}$ 0.12 if $T > T_{liquidus}$
4	Viscosity (Ns/m^2)	–	$0.001 \times exp(-4.25 + 1790/T)$
5	Thermal expansion coefficient β (1/K)	1.67×10^{-5}	5×10^{-4}
6	Latent heat (J/kg)	–	173,400
7	Solidus temperature (K)	–	319
8	Liquidus temperature (K)	–	321

Table 2
Maximum temperature after 400 s of computational time and % deviation for a deep domain with top wall heating.

Grid size	Maximum temperature after 400 s	% Deviation
100 × 80	1029.91	0.1754
100 × 90	1031.09	0.0610
110 × 100	1031.27	0.0436
150 × 120	1031.72	Base value

2.1. Numerical study of composite phase change materials

A numerical study is carried out in order to identify the flow

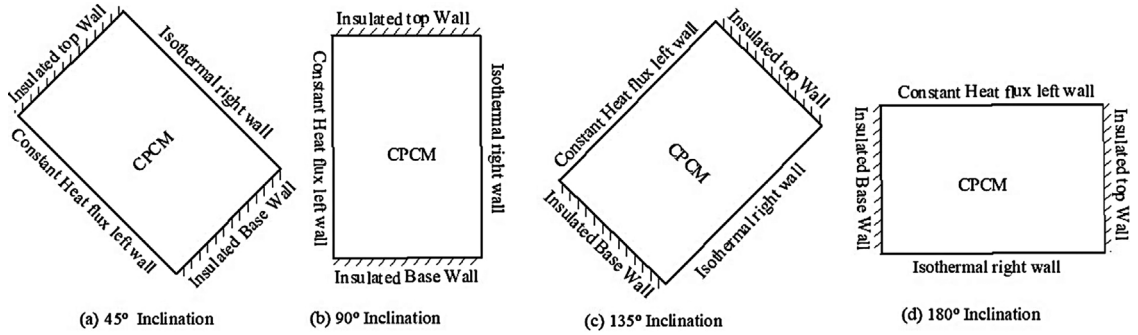

Fig. 1. Geometrical representation of 2-D model with different orientations.

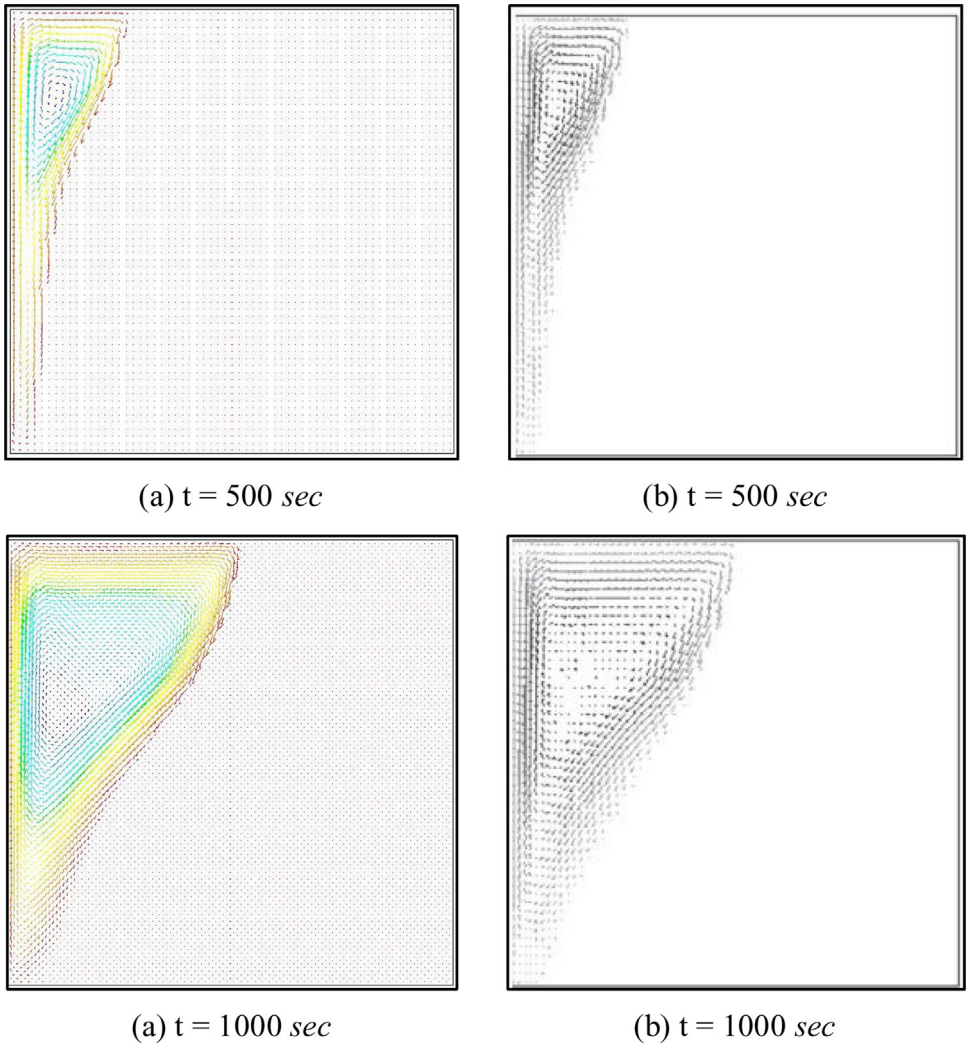

Fig. 2. Streamline patterns of results: (a) present results and (b) results of [19].

patterns and heat transfer parameters.

The governing conservation equations [19] are as follows:

Continuity equation:

$$\frac{\partial \rho}{\partial t} + \nabla\cdot(\rho\vec{U}) = 0 \tag{1}$$

Momentum equation:

$$\frac{\partial}{\partial t}(\rho\vec{U}) + \nabla\cdot(\rho\vec{U}\vec{U}) = -\nabla P + \rho\vec{g} + \nabla\cdot\vec{\vec{\tau}} + \vec{F}, \tag{2}$$

where P is the static pressure, $\vec{\vec{\tau}}$ is the stress tensor, and $\rho\vec{g}$ and $\vec{F}$ are the gravitational body force and external body forces, respectively.

Energy equation:

$$\frac{\partial(\rho H)}{\partial t} + \nabla\cdot(\rho\vec{U}H) = \nabla\cdot(K\nabla T) + S, \tag{3}$$

where H is the enthalpy of the CPCM, T is the temperature, ρ is the density of CPCM, K is the thermal conductivity of CPCM, $\vec{U}$ is the velocity and S is volumetric heat source term.

2.2. Thermophysical properties

The thermophysical properties of base PCM (Paraffin wax) and nano additives (Cu nanoparticles) are given in Table 1. The difference between the solidus and liquidus temperatures represents the mushy zone during the melting of CPCM. The temperature dependent properties such as, density, specific heat capacity, latent heat, dynamic viscosity and thermal conductivity of the CPCM is defined as follows [19]:

$$\rho_{cpcm} = \varphi\rho_{np} + (1-\varphi)\rho_{pcm}, \tag{4}$$

$$Cp_{cpcm} = \frac{\varphi(\rho Cp)_{np} + (1-\varphi)(\rho Cp)_{pcm}}{\rho_{cpcm}}, \tag{5}$$

$$L_{cpcm} = \frac{(1-\varphi)(\rho L)_{pcm}}{\rho_{cpcm}}, \tag{6}$$

$$\mu_{cpcm} = 0.983e^{(12.959\varphi)}\mu_{pcm}, \tag{7}$$

$$K_{cpcm} = \frac{K_{np} + 2K_{pcm} - 2(K_{pcm} - K_{np})\varphi}{K_{np} + 2K_{pcm} - 2(K_{pcm} - K_{np})\varphi}K_{pcm} + 5\times 10^4\beta_k\zeta\varphi\rho_{pcm}Cp_{cpcm}\sqrt{\frac{BT}{\rho_{np}d_{np}}}f(T,\varphi), \tag{8}$$

where B is Boltzmann constant, $1.381\times10^{-23}J/K$ and $\beta_k = 8.4407(100\varphi) - 1.07304$

f (T, φ) $= (2.8217\times10^{-2}\varphi + 3.197\times10^{-3})\ T/T_{ref} + (-3.0669\times10^{-2}\varphi - 3.91123\times10^{-3})$where T_{ref} is the reference temperature = 273 K, and ζ is the correction factor and its value are the same as value for liquid fraction β.

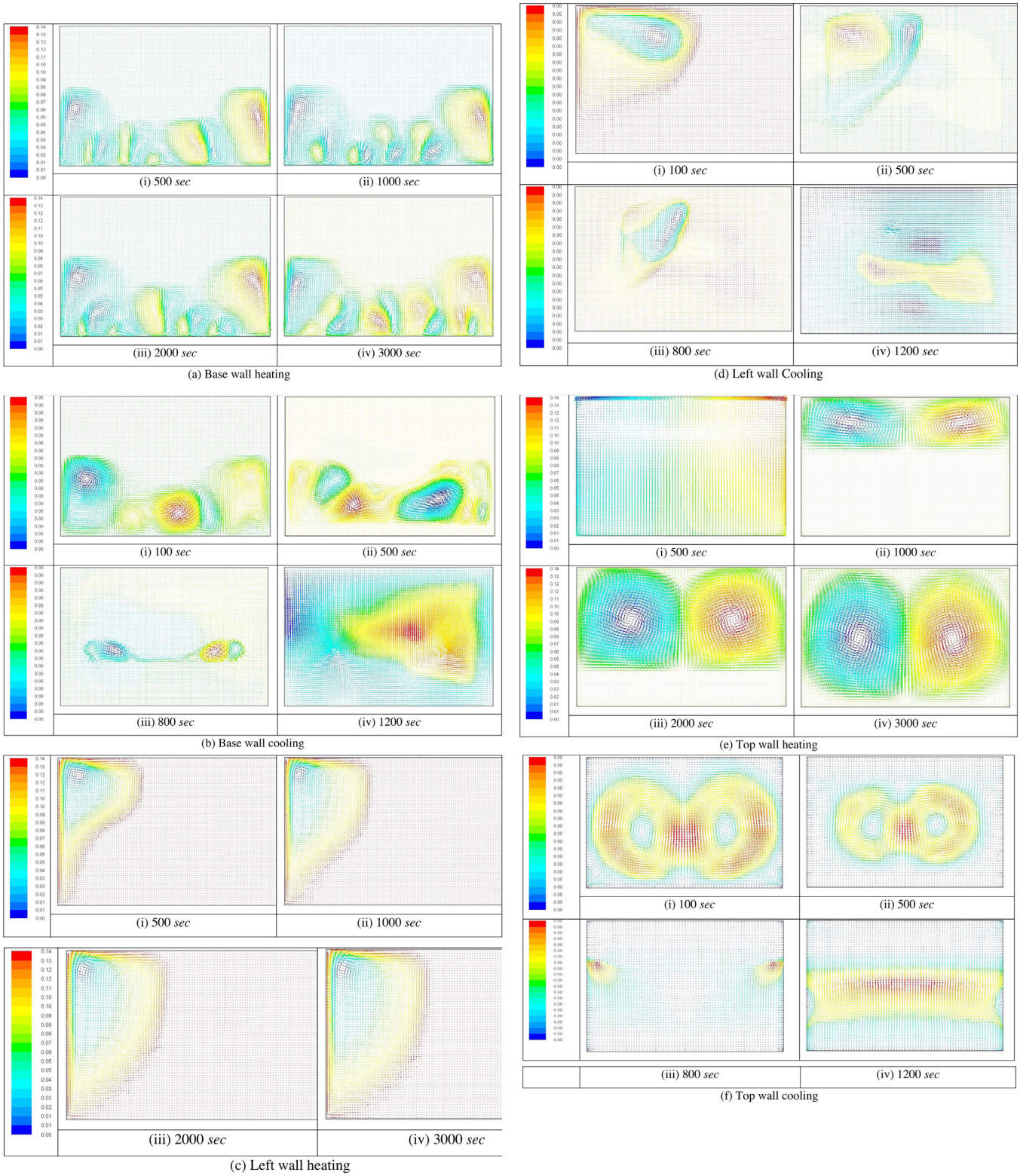

Fig. 3. Flow characteristics of the shallow domain in which (a), (c) and (e) show the heating process and (b), (d) and (f) show the cooling process.

2.3. Boundary conditions

The numerical study is carried out for four different orientations by imposing the constant heat flux at one wall and the opposite wall is isothermal conditions at 300 K to the opposite wall and remaining walls are insulated.

(i) Constant heat flux applied to base wall;
(ii) Constant heat flux applied to left wall;
(iii) Constant heat flux applied to top wall.

All four orientations cases are investigated and observed the factors which are significantly affecting the melting/solidification process.

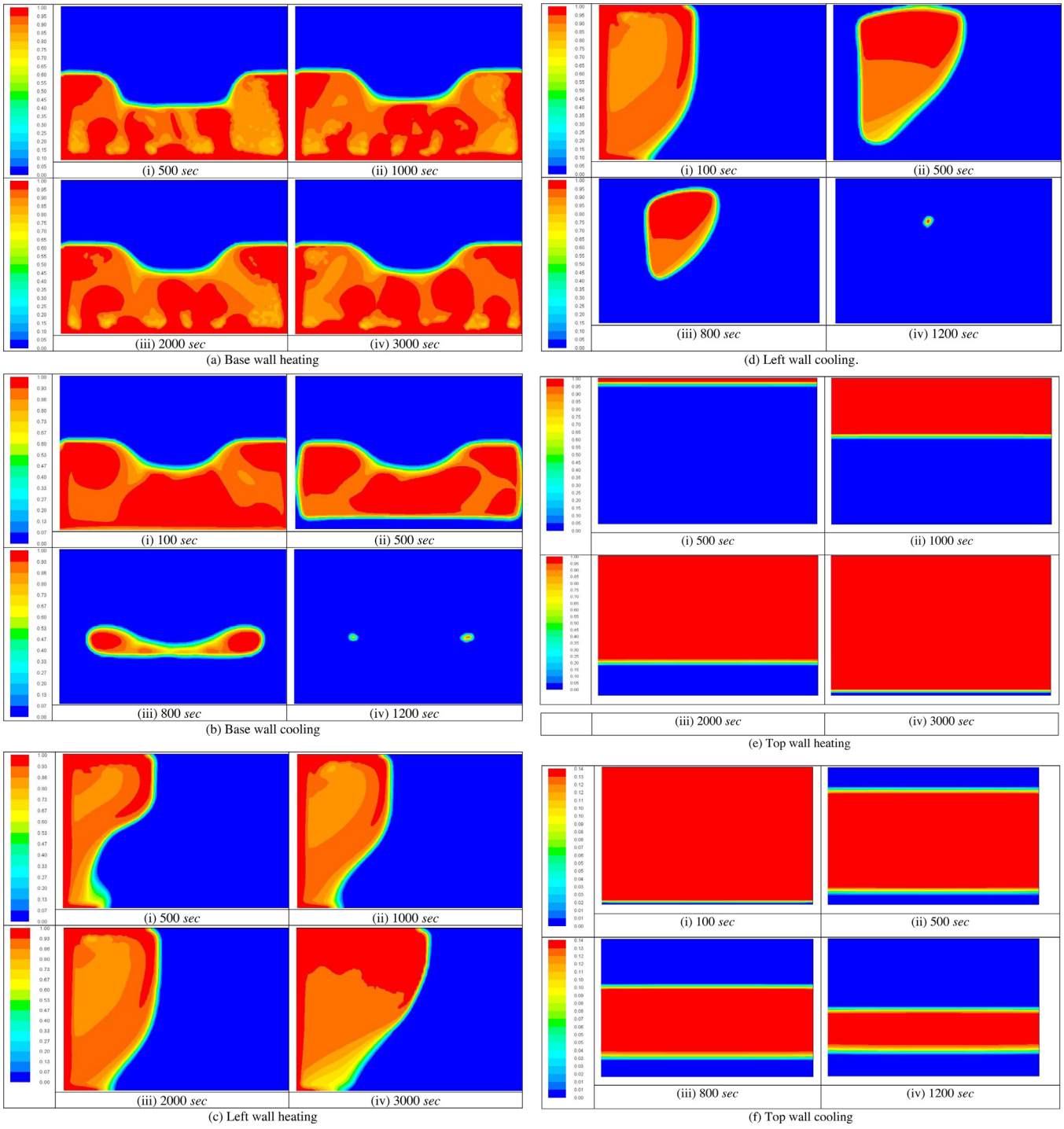

Fig. 4. variation of melting fraction for the shallow domain in which (a), (c) and (e) heating process and (b), (d) and (f) cooling process.

2.4. Computational procedure

The geometrical model with aspect ratio 1.5 (ratio of length to width) is modeled using pre-processor software ICEMCFD 15.0. A good quality mesh is generated for superior results, near the boundaries fine structured mesh is generated to compensate computational domain and resolve the boundary layer conflicts. Increasingly fine mesh generated in the rest of domain to minimize the computational time. The meshed model is imported to FLUENT 15.0 for solving the governing equations. In the present work PRESSURE BASED method is adopted for solving governing equations and all the thermophysical properties of CPCM are defined by using user-defined functions (UDF). FIRST ORDER upwind differencing scheme is used, and PRESTO scheme is adopted for pressure correction. The under-relaxation factors for the pressure correction, velocity components and thermal energy are 0.3, 0.5 and 1.0 respectively. Convergence criteria are 10^{-6} for continuity and momentum equations and 10^{-9} for energy equation. Enthalpy-porosity technique is used to study the melting/solidification process.

2.5. Grid Independent study

A detailed grid sensitivity analysis is carried out in order to find the optimum grid size for the computational analysis. The maximum temperature obtained in the present numerical study is selected for each

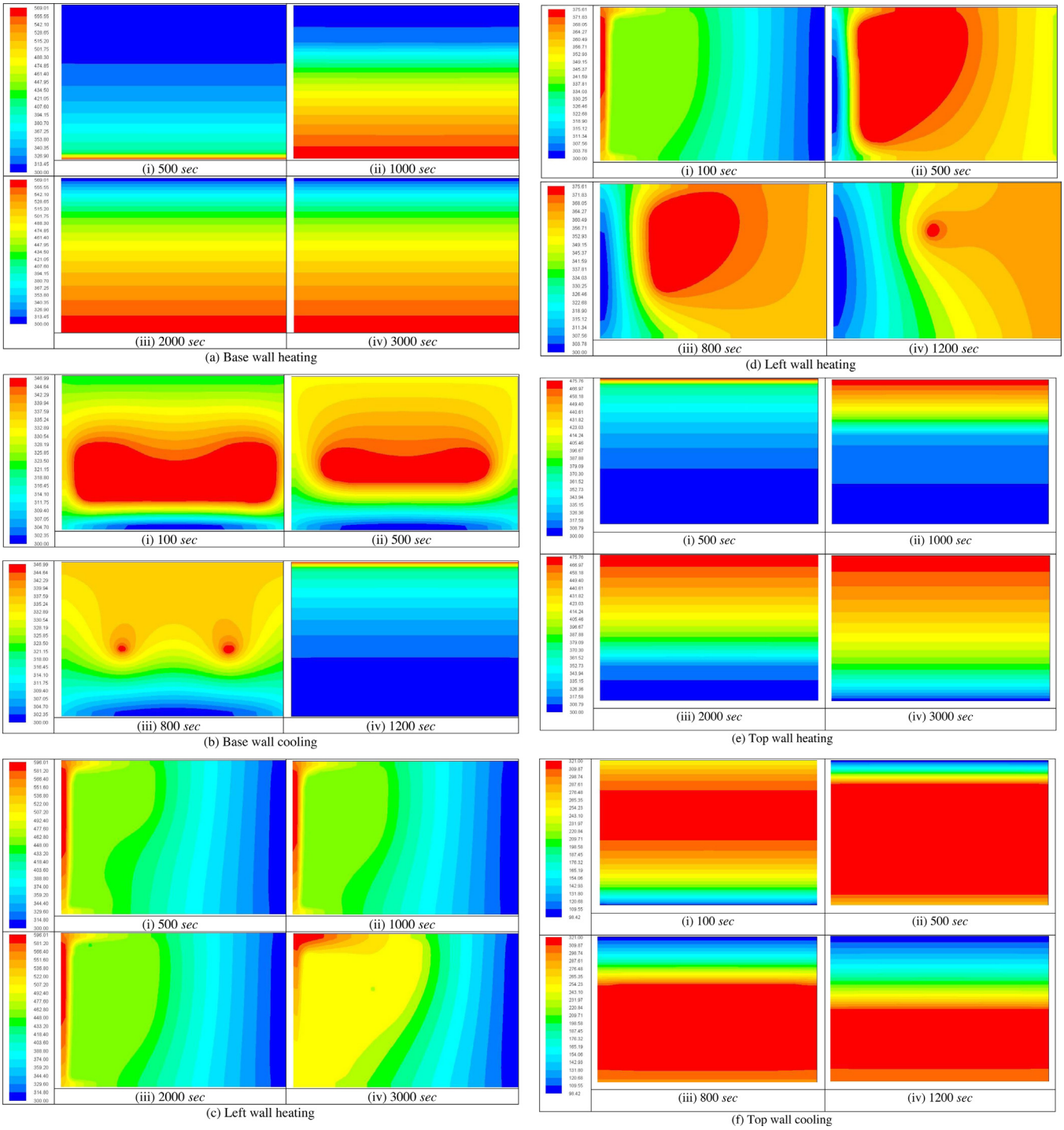

Fig. 5. variation of temperature for the shallow domain in which (a), (c) and (e) shows the heating process and (b), (d) and (f) shows the cooling process.

grid and results are tabulated. Table 2 shows maximum temperature after 400 s of computational time and percentage deviation from the base value for a deep domain with top wall heating.

From Table 2 it is clear that the grid size of 110 × 100 shows the least deviation on maximum temperature compared to other three sizes, so grid size of 110 × 100 is selected as an optimal grid for further numerical computations.

2.6. Numerical model validation

The present work is validated with the Khodadadi et al. [19], CPCM (98% Paraffin wax and 2% of Al_2O_3 nanoparticles) is used and the results are compared for two different time durations of 500 and 1000 s [19]. Fig. 2 shows the streamline patterns of present results. The boundary conditions imposed as, left wall at a constant temperature of 330 K, the right wall at 300 K, and remaining top and bottom walls are insulated and results shown good agreement.

3. Results and discussion

The complete melting and solidification processes are divided into different time steps (500, 1000, 2000 and 3000 s) for melting and (100, 500, 800 and 1200 s) solidification respectively to understand the mechanism. Maximum time limit 3000 s is selected because shallow

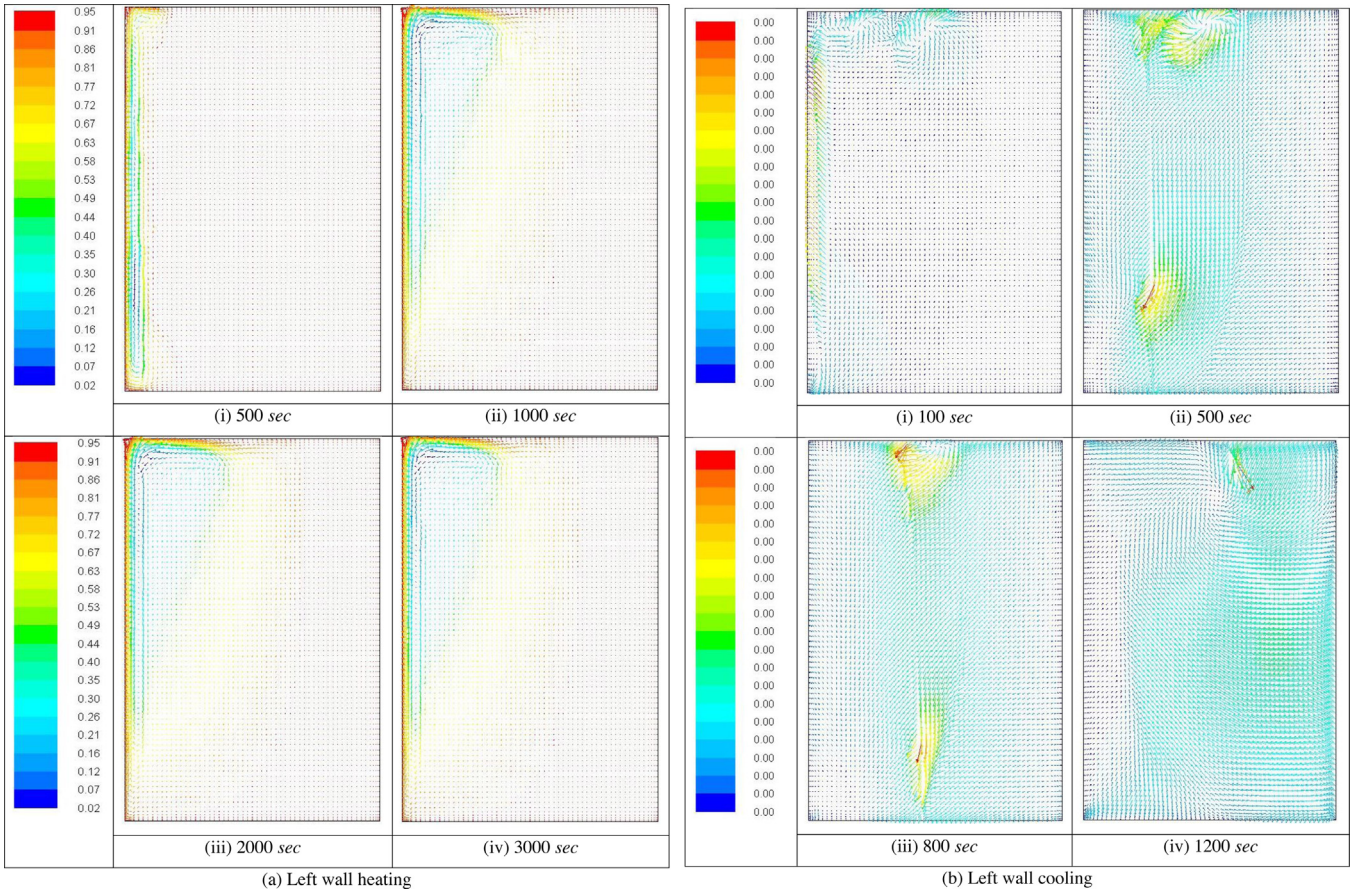

Fig. 6. Flow characteristics of top wall: (a) heating and (b) cooling in the deep domain.

domain completed melting at 3000 s and it is considered for comparison. Solidification also completes in 1200 s. Orientation effects are studied for flow characteristics, melting of CPCM and temperature distribution.

3.1. Shallow geometry (180° orientation)

3.1.1. Flow characteristic study

Flow characteristic variation for base wall heating and cooling is shown in Fig. 3(a) and (b) respectively. Heat transfer through base wall forms circulation vortices adjacent to the hot wall, which is due to the development of the melting front. The progression of buoyancy effect causes the development of circular currents adjacent to the hot wall of domain. A sunken shape at the upper section of the melt front is observed while in the upper portion of domain interface is linear. For 3000 s of time duration, it covers only half of domain and there is no change in the streamline patterns due to non-penetration of melting layer. Heat extraction reduces the vortex formation during solidification process as time progresses, these patterns disappear and generate a uniform distribution of streamline profile at time duration of 1200 s.

Flow characteristic variations for left wall heating and cooling are shown in Fig. 3(c) and (d) respectively. In the melting process streamline patterns forms a thin layer of molten CPCM near the hot wall, which demonstrates the conduction mode of heat transfer and it succeeds until the fluid is resisted by the viscous effect. At this stage, the solid-liquid interface becomes steady and remains uniform along the surface of the hot wall. As time progresses, melt layer thickness builds and buoyancy effect increase which dominates the viscous effect. The top portion of the solid-liquid interface initiates the natural convection currents in the melting region and starts dissolving due to erosion. The increase in buoyancy effect develops the circulating currents and the bottom portion of domain of melt front changes and raises with time.

Flow characteristic variations for top wall heating and cooling are shown in Fig. 3(e) and (f) respectively. In the early stages of melting, streamline patterns changes abruptly and as temperature varies, the convection currents travel and occupies the significant portion of domain. The impact of viscous effect against domain walls diminishes, along these lines permitting the liquid to rise. The smooth movement of fluid develops continuously until 3000 s. The natural convection currents in domain are fully generated and the complete process can be visualized in Fig. 3.

3.1.2. Melting of composite phase change material

The contours in Fig. 4 show the melting fractions from the base wall heating in the shallow domain. At the beginning of the melting process, the solid-liquid interface dominated by conduction. Subsequently, the interface patterns change to the wavy structure and controlled by the natural convection streams in the liquid CPCM. The hot liquid CPCM travel toward the center of domain in the opposite direction to the hot wall due to erosion, the solid CPCM falls to the bottom of domain as shown in Fig. 4.

As the fluid layer builds toward the center and vanishes, but the liquid fraction at the base wall increases. The molten liquid ascents through the vertical walls and tumbles from the center of domain and variation of melting fraction during base wall heating and cooling are shown in Fig. 4(a) and (b) respectively. Approximately half portion only gets melted due to lack of contact between molten and the solid phase. Thin molten layers cannot penetrate at higher level because conduction gets depressed and the convection dominates. The heat transfer coefficient becomes very small and convection becomes insignificant. The effect of gravity on molten phase causes settlement on the base wall and buoyancy effect is not sufficient to reach out the remaining portion of

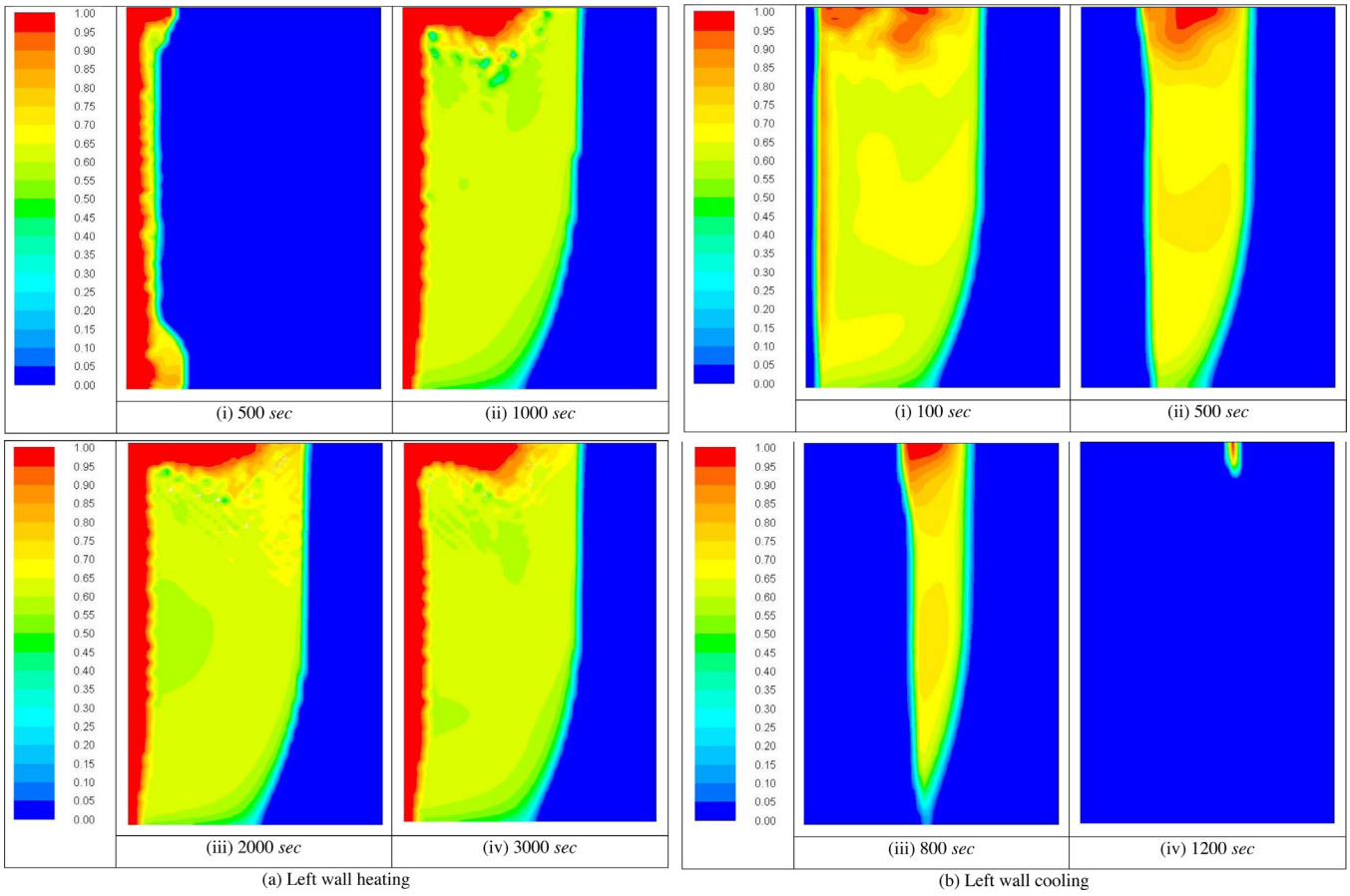

Fig. 7. variation of meting fraction for top wall: (a) heating and (b) cooling with time in deep domain.

domain. The orientation affects melting/solidification process, shallow domain shows the fastest melting rate as compared to other orientations at the early stage of melting process. The molten fluid is fallen and spread all over the solid CPCM and it comes directly in contact with solid. Heat transfer begins and covers a larger surface area of solid CPCM and melts relatively faster. The uniform melting can be achieved and complete melting without partially molten patches.

The solidification process is dominated by conduction and the orientation significantly affects melting process due to the variation of natural convection currents and gravitation effect. Conversely, the inclusion of nano-additives, such as copper or copper oxide nanoparticles, might significantly depress the natural convection heat transfer rate and reduce the melting process when orientation is changed and the same trend are observed in previous studies [20].

Melting fraction variation during left wall heating and cooling is shown in Fig. 4(c) and (d) respectively. In the left wall heating case, interface movement is uniform and profile at the upper region is smoothly curved at the beginning and expands slightly. The higher melting rate at the upper part of domain where the fluid CPCM ascended along the heated wall. The melting rate is low at the bottom of domain where fluid usually is cold. Compared to all other cases, this case takes longer duration of time to complete the melting process, up to 3000 s only small portion of CPCM is melted but cooling occurs at much faster rates. The domination of the conduction since molten fluid is fallen and spread all over the solid CPCM. In this circumstance molten fluid comes directly in contact with solid and heat transfer begins, hence CPCM melts quickly.

Melting fraction variation during top wall heating and cooling are shown in Fig. 4(e) and (f) respectively. The heat transfer coefficient becomes very low and convection becomes insignificant. The effect of gravity on molten phase causes settlement on the base wall and hence buoyancy effect is not sufficient to reach out the remaining portion of domain. The solid-liquid interface becomes steady and uniform along the surface of hot wall. As time progresses and the melt layer thickness builds, the increase in buoyancy effect dominates viscous effect. The top portion of the solid-liquid interface initiates the natural convection currents in the melting region and starts dissolving due to erosion. Unlike in the melting process the solidification occurs in the faster way due to reconnection and accumulation of eroded dissolved particles. Solid phase formation is quicker at the upper portion of domain and rejects heat from the mushy zone. As the solid CPCM shrinks and its pinnacle point moves down along the left wall the temperature of molten CPCM at the top portion of domain expands which affirms the contiguity of the ineffective velocity field. Besides, the growth of molten CPCM at the top part of domain discloses that a significant bit of the heat absorbed by molten CPCM from the heated wall. Moreover, it indicated the upper part of domain without solid CPCM [21]. The complete process with different wall heating can be visualized in Fig. 4.

3.1.3. Temperature distribution

Initially temperature patterns are almost parallel to the heating wall and heat transfer predominant inside the shallow domain. At a later stage the temperature of the liquid CPCM near the heating wall increases and molten CPCM travels along vertical sides due to a succession of buoyancy effect over the viscous force. Temperature distribution patterns for base wall heating and cooling process are shown in Fig. 5(a) and (b) respectively. The liquid CPCM travels until it reaches the upper portion of domain and diverts toward the solid region, the impingement of molten CPCM enhances the local heat transfer coefficient and hence melting rate increases subsequently. The melting rate at the bottom portion of domain is significantly lower compared to the upper part. This indicates the temperature reduction of molten CPCM as

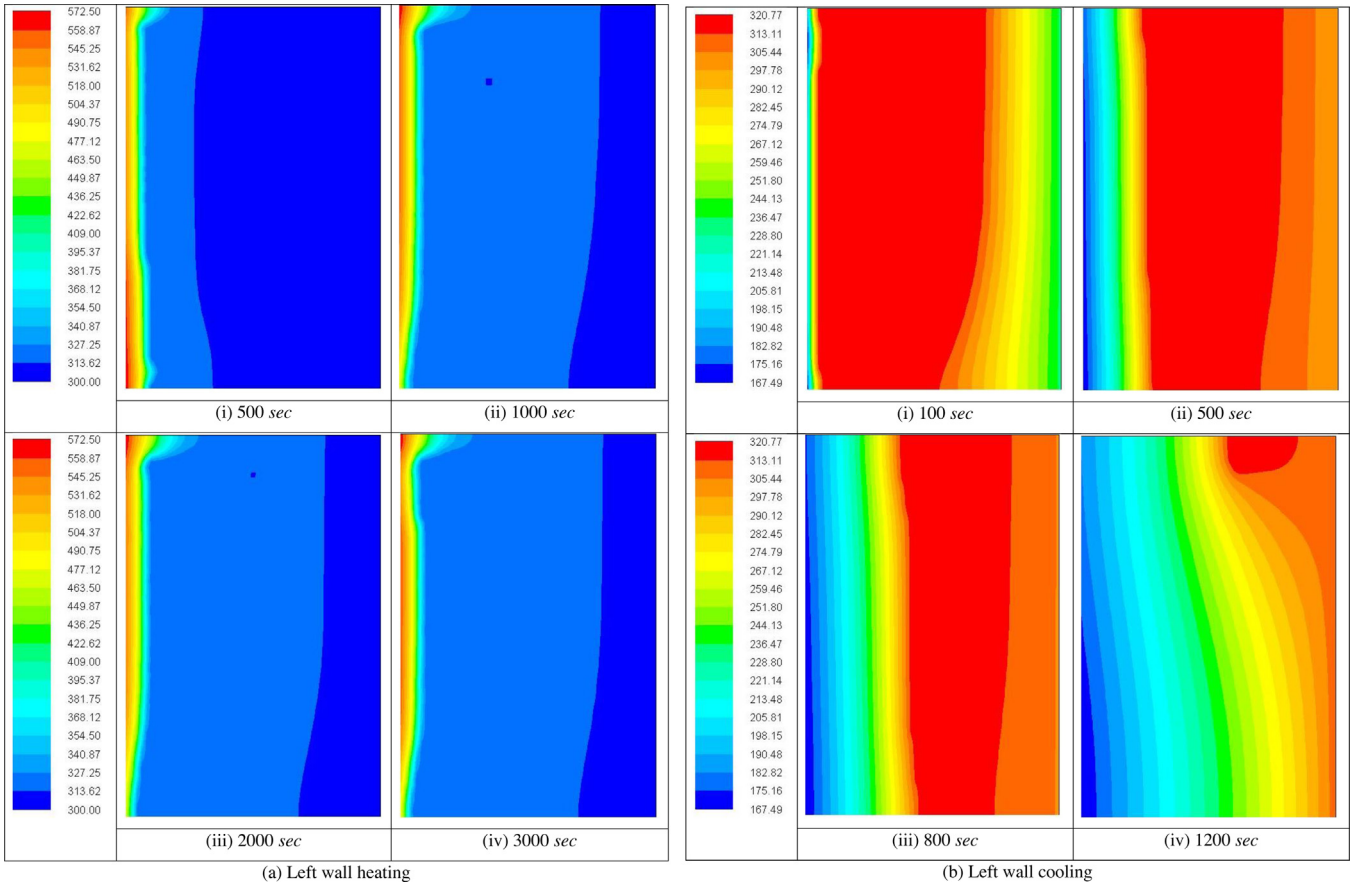

Fig. 8. Variation of temperature for top wall: (a) heating and (b) cooling with time in the deep domain.

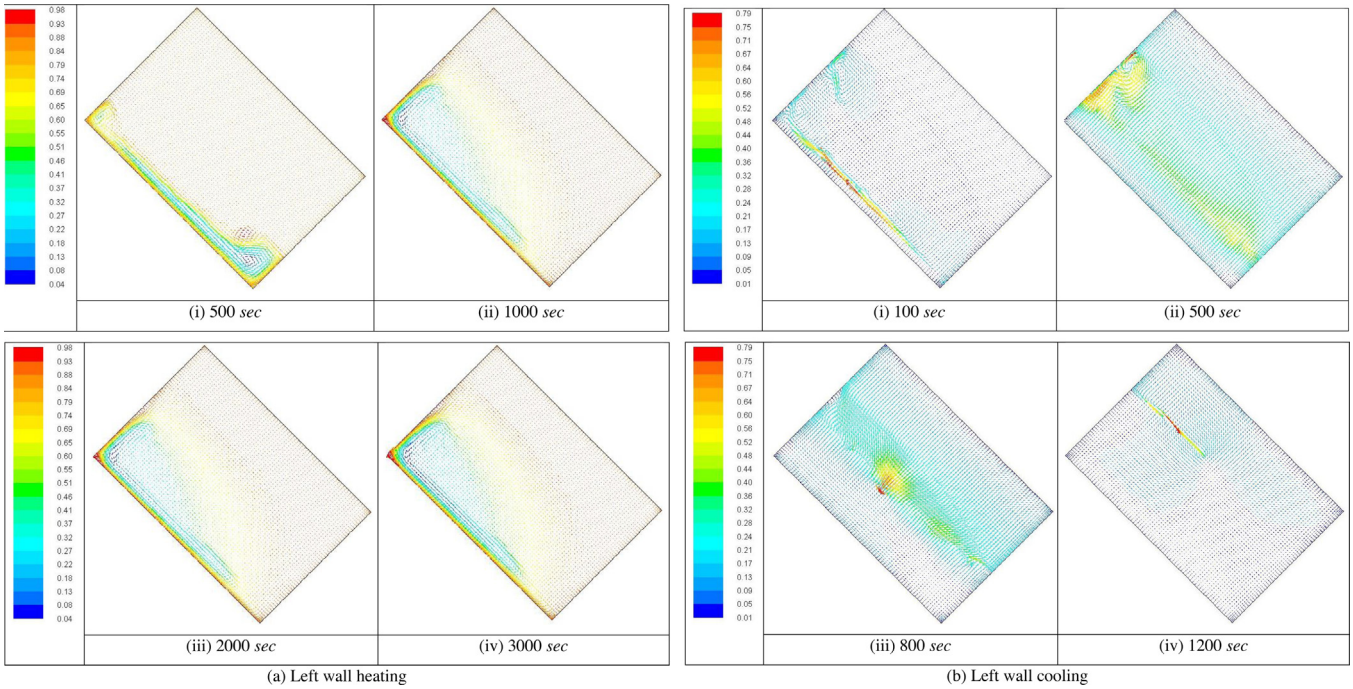

Fig. 9. Flow characteristics of the left wall: (a) heating and (b) cooling for 45° orientation.

it drops along the interface and results in lower heat transfer to the solid CPCM.

As the solid CPCM shrinks and its pinnacle point moves down along the left wall the temperature of molten CPCM at the upper portion of domain expands which affirms the contiguity of the ineffective velocity field. Besides, the buildup of molten CPCM at the upper part of domain discloses that a significant bit of the heat absorbed by molten CPCM from the heated wall. Moreover, it indicated the upper part of domain

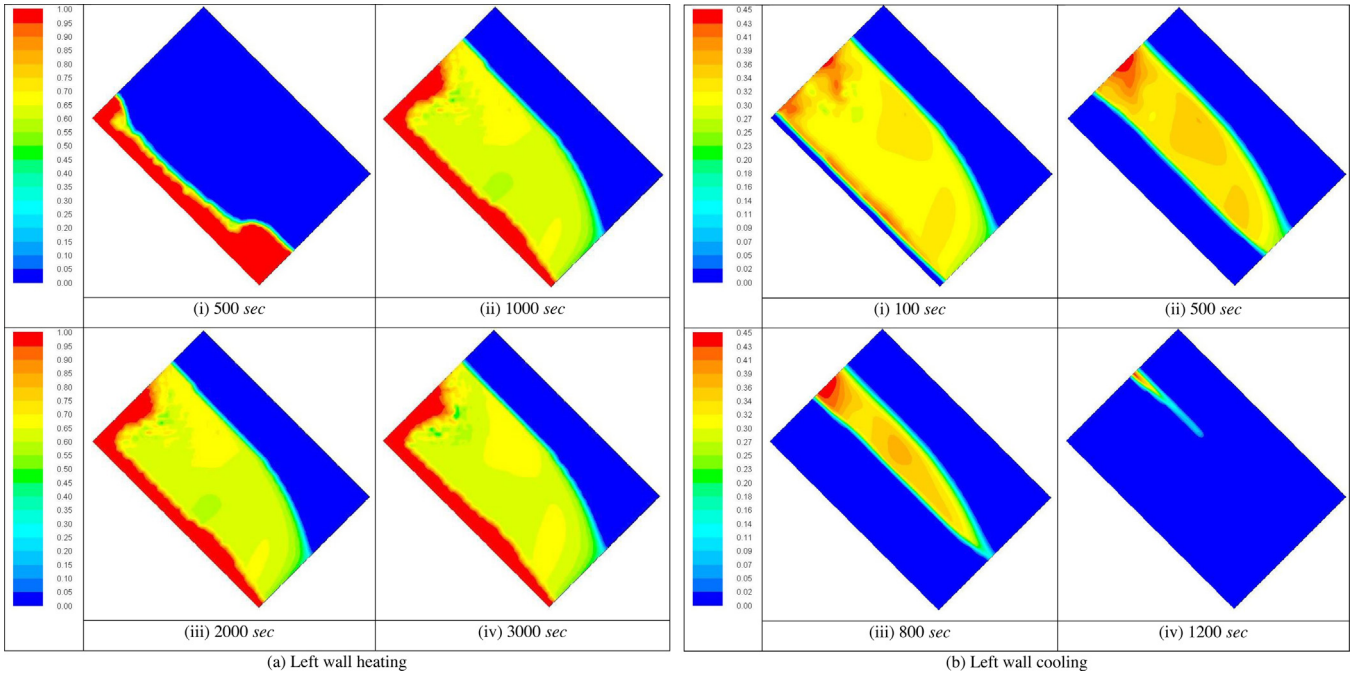

Fig. 10. Variation of melting fraction for left wall: (a) heating and (b) cooling for 45° orientation.

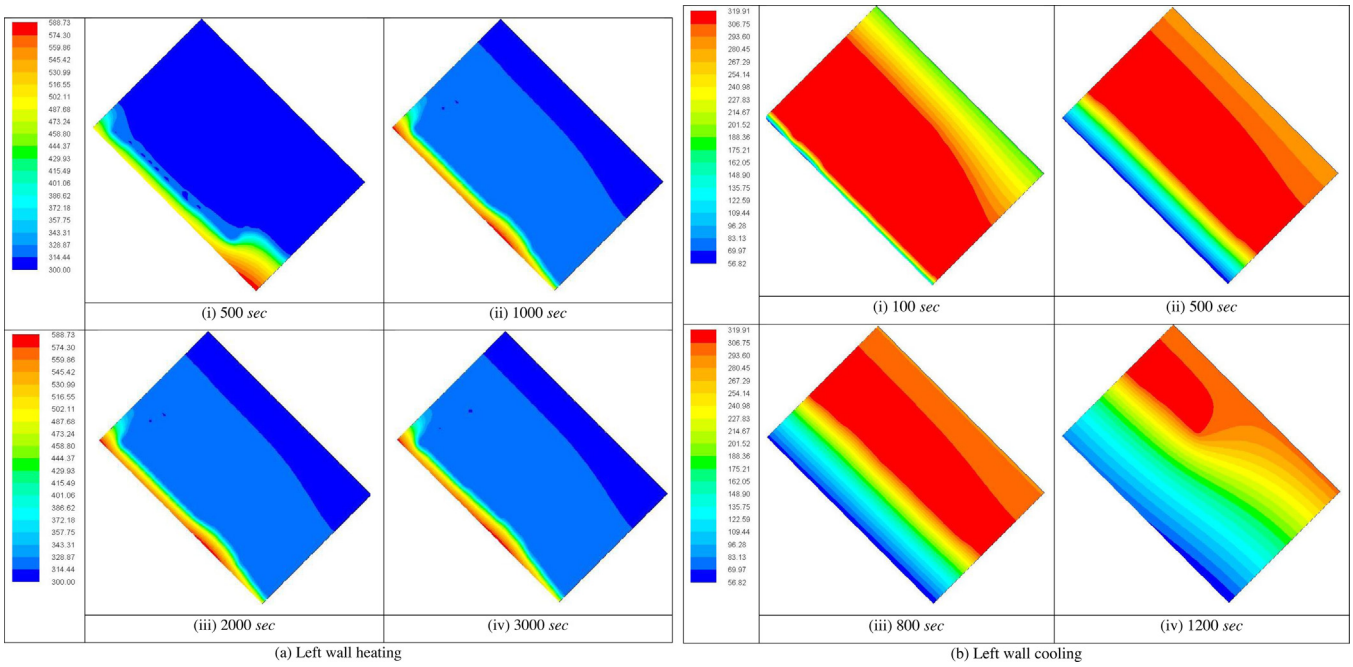

Fig. 11. Variation of temperature for base wall: (a) heating and (b) cooling for 45° orientation.

without solid CPCM. In this area, molten CPCM assembles on the cold more massive liquid layers bringing about the advancement of stratified liquid layers. Temperature profile replicates the isothermal wall because heat has not reached till that point and it remains in sub-cooled form with a uniformly distributed temperature profile. Fig. 5(c) and (d) shows temperature distribution patterns for left wall heating and cooling process respectively. During the solidification process the temperature patterns change completely, at initial phases surrounds molten CPCM which act like heat source through which heat distributed gradually. The size of this region gets reduced and at the completion of the process it disappears completely.

The left wall heating provides a uniform temperature distribution profile all over the surface of domain. The temperature contours are almost linear with the heating wall and it carried to the base wall which is exposed to the ambient. Temperature distribution patterns for top wall heating and cooling process are shown in Fig. 5(e) and (f) respectively. Other than the sub-cooled region the contours are uniform and impingement of molten CPCM to the solid-liquid interface quickens the melting rate. The melting rate at the lower portion of domain is substantially less than that of the upper parts. This can be clarified by the way that the temperature of molten CPCM reduces as it falls along the interface and results in lower heat transfer to the solid CPCM at the lower parts of domain. The complete process for different heating cases can be seen from Fig. 5 variation of temperature for the shallow domain

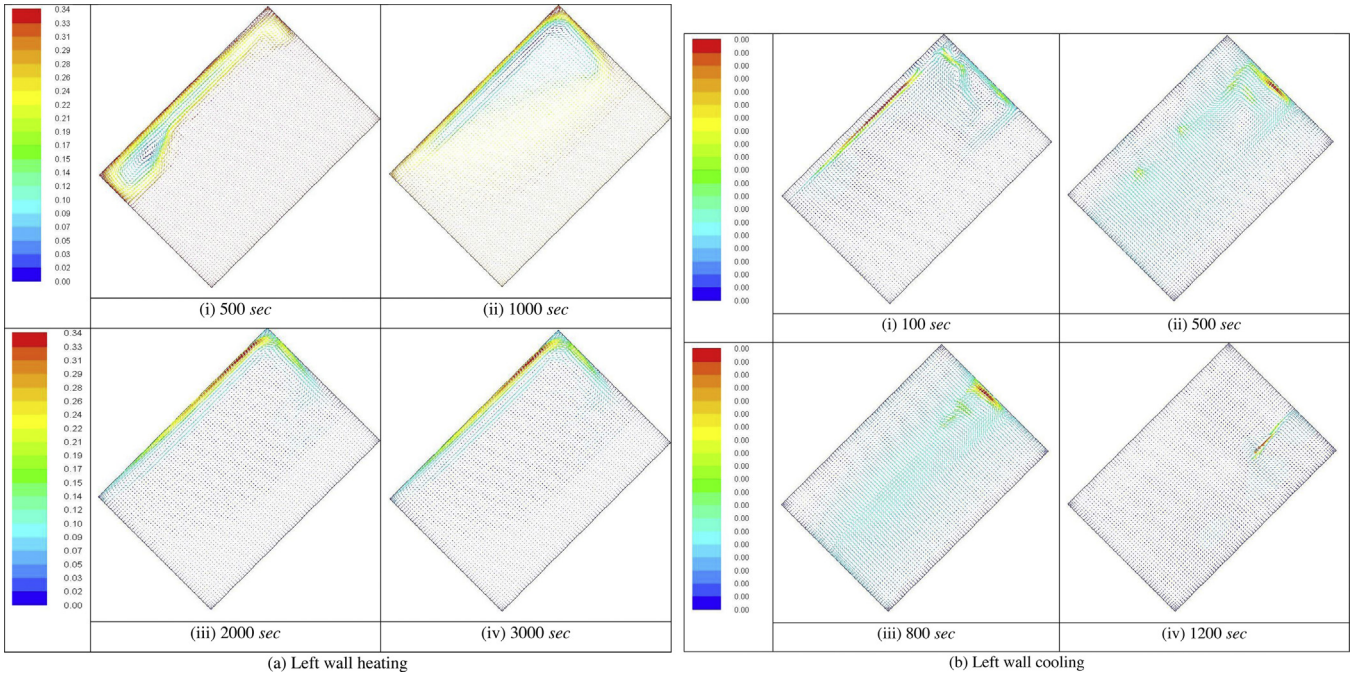

Fig. 12. Flow characteristics of the left wall: (a) heating and (b) cooling in 135° orientation.

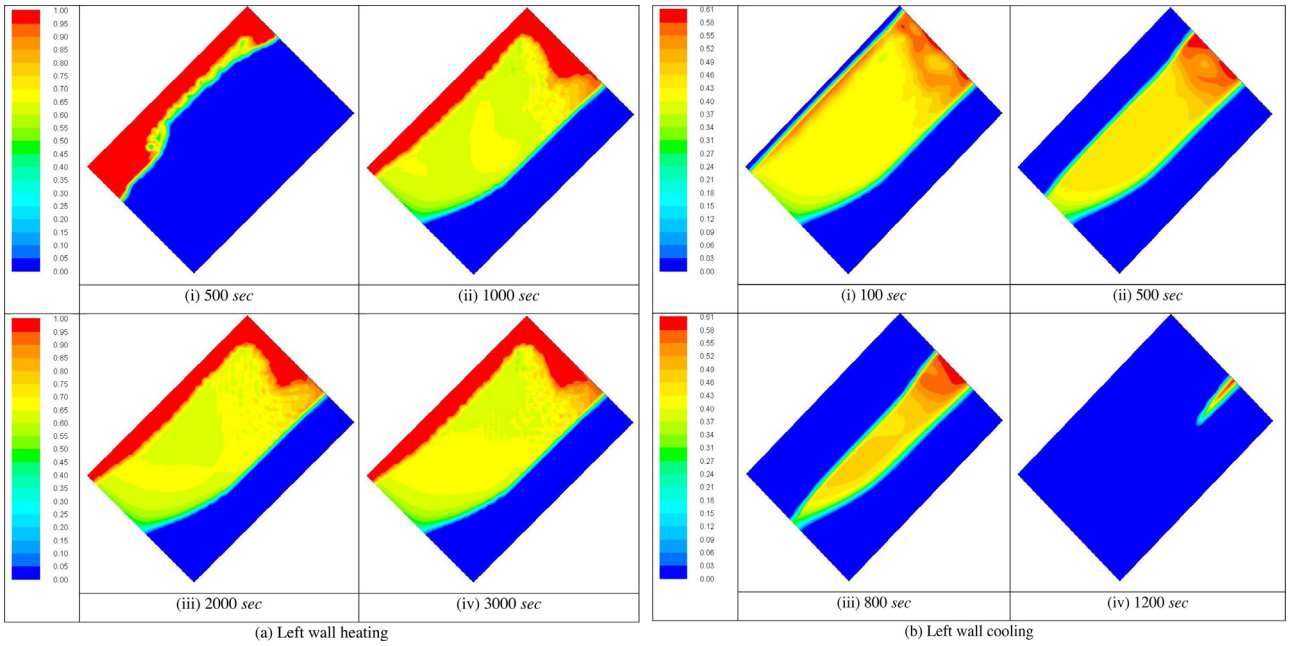

Fig. 13. Variation of melting fraction for left wall: (a) heating and (b) cooling with time in 135° orientation.

in which (a), (c) and (e) shows the heating process and (b), (d) and (f) shows the cooling process.

It is known that, heating from the top surface is an efficient way to achieve faster melting/solidification. During solidification, the solid phase formation is also much quicker due to the availability of high area of exposure. Heat transfer through base wall makes streamlines patterns to form circular vortices adjacent to the hot wall, which is purely due to the development of melting front and movement of fluid flow velocities. The progression of buoyancy effect causes the growth of circular currents at adjacent to the hot wall of domain, making a sunken shape at the upper section of the melt front while in the upper portion of domain the interface is linear. A consistent change in the melting layer thickness and average variation in patterns of the solid–liquid interface shows the development of a prodigious flowing current in the liquid shown. For the sufficient time duration, it covers only half of domain and there is no change in the streamline patterns due to non-penetration of melt layer. Heat extraction process reduces the vortex formed during the melting process, as time progresses these patterns start disappearing and a uniform velocity distribution profile generates.

3.2. Geometry orientation at 90°

3.2.1. Flow characteristic study

The flow characteristics pattern variations for 90° orientation are shown in Fig. 6. In the melting process, the flow patterns move toward the entire bounded domain, which results in faster heat transfer rate.

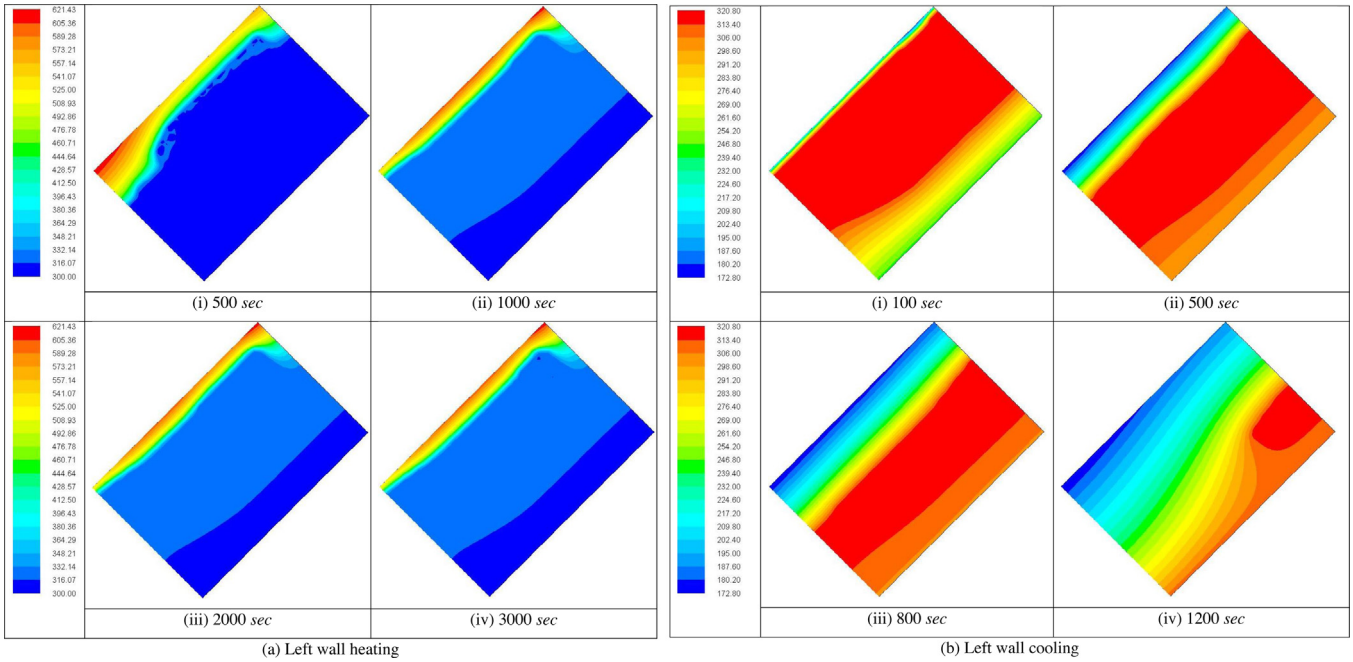

Fig. 14. variation of temperature for left wall: (a) heating and (b) cooling with time in 135° orientation.

During the initial phase of the melting process the melting rate is very high, due to the high temperature difference between molten and solid CPCM. As time progresses the heat transfer rate drops and therefore, heat flux reduces and the melting process sojourns with uniformly distributed streamline patterns. Before the start of the solidification process the CPCM is in molten state and circulates inside domain completely by occupying the whole domain. In solidification process flow patterns breaks and spreads the whole domain, which indicates the complete solidification of the CPCM and completion of the solidification process.

This flow is a consequence of the natural convection which has happened due to the temperature difference between molten phase and the solid phase of the CPCM. Given the significant temperature difference during solidification the buoyancy effect increments quickly and this causes the molten region to solidify faster by increasing solid layer thickness. Continuous reduction of the molten region reduces the mass fraction and streamline vectors slowly spreads all over domain [22].

3.2.2. Melting of composite phase change material

In the initial stages of the melting process, the liquid interface imitates the profile of the hot wall due to the domination of conduction heat transfer in the melt zone. The viscous effect opposes the fluid motion and succeeds the conduction with a uniform melting profile. As the process continues, the liquid fraction increases and spreads all over domain. As molten fluid starts flowing downwards along the interface heat transfer takes place from hot molten fluid to solid CPCM. Because of this, the melting rate is much higher at the upper portion of domain as shown in Fig. 7. The heat interaction between the thin molten layer to the thick solid CPCM is much quicker due to overlapping of complete solid surface.

The dominant circulating currents are formed due to the consistent variation of melt layer thickness and changing phase from solid to liquid. As time succeeds, similar patterns retain until CPCM completely gets melted. In the cooling process solidification begins from both hot and cold wall by concentrating molten phase in the center, continuous growth of solid phase makes patterns to shrink and finally gets dissolves by completing the cooling process.

3.2.3. Temperature distribution

The temperature is non-uniformly distributed all over the surface of domain other than the sub-cooled region. At heated upper portion the temperature is naturally high and traveled with a gradual decrease through the vertical walls shown in Fig. 8. Unlike the other two heating cases top wall heating gave a uniform temperature distribution for complete melting and solidification process. These uniform patterns indicate the proper melting and traveling of uniform melting front.

3.3. Geometry orientation at 45°

3.3.1. Flow characteristic study

The flow characteristics for all the three wall heating cases are studied, the flow characteristic study showed a uniform distribution of streamlines. The heat transfer mechanism adjacent to the hot wall is purely by conduction and the CPCM starts to absorb the heat and initiates the meting process. Once it reaches the saturation limit, immediately begins to change its physical state and forms a liquid layer over the solid surface. The molten layer gets separated from the hot wall and convection plays a vital role.

Further heat transfer takes place only through the convection mode molten liquid CPCM flows in a downward direction due to the effect of gravity and melting process gets accelerated, movement of flow vectors can be visualized from Fig. 9. A consistent change in the melting layer thickness and average variation in patterns of the solid-liquid interface shows the development of a significant flowing current in the liquid PCM [23].

The melt front showed articulated bulge along the hot wall due to the impact of the convection in the mushy zone. The streamline patterns are too far from the cold wall, this increases the heat loss and increases the bulge size in the cooling region. In meantime, the returning streamline patterns from the hot wall impede development of the mushy zone at the upper portion of domain making bulge more intense at the center. At the initial stages the flow field is slightly close to the hot wall because of the no-slip condition of walls. Thus, remarkable solidification occurs around there, at a later stage, more significant moment of the liquid creates higher flow fields near the hot wall and solidification proceeds. The solidification behavior is observed for the transient transformation of the flow field. Finally, the circular

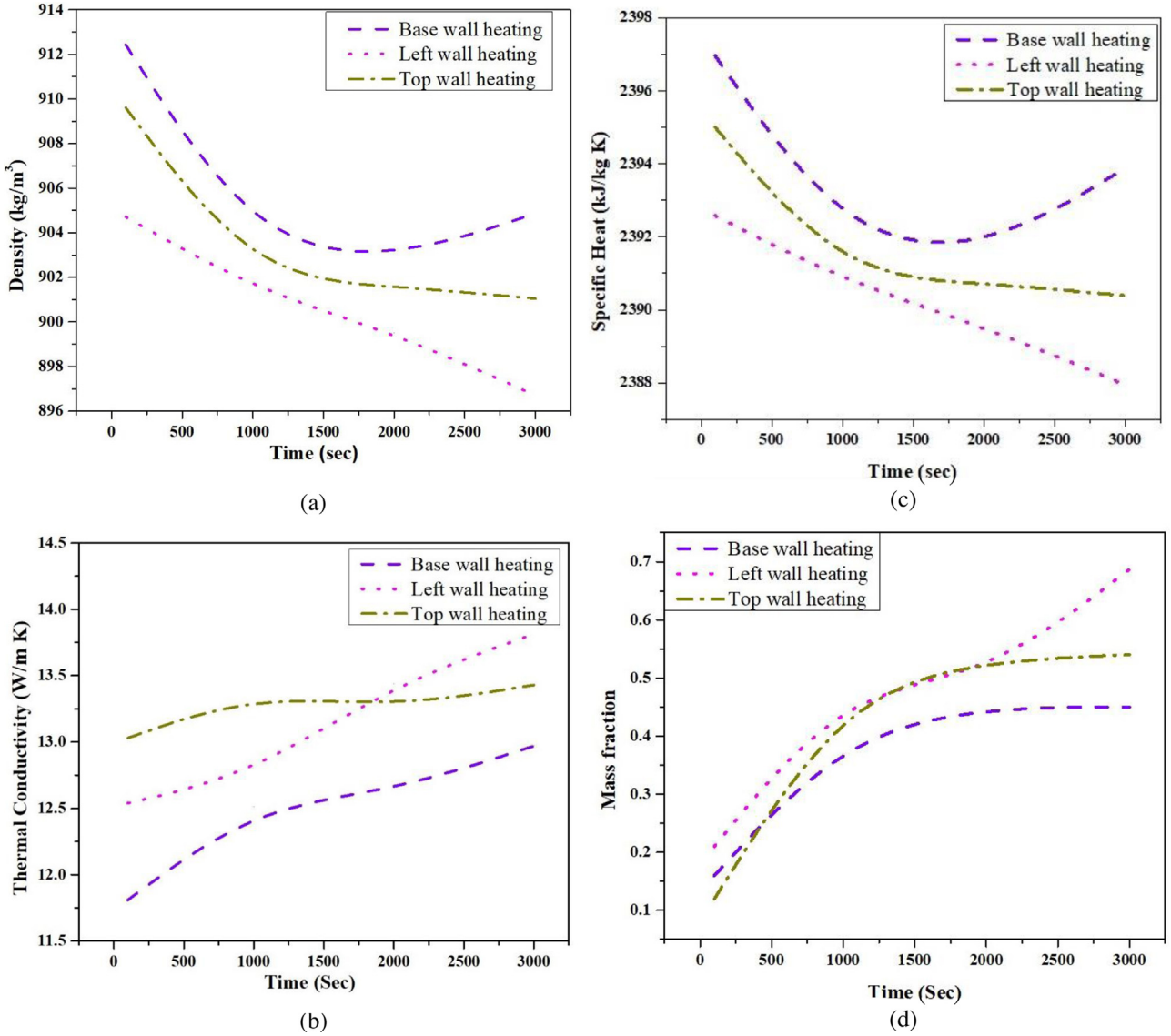

Fig. 15. Thermophysical properties variation in 45° orientation for different wall heating: (a) density, (b) thermal conductivity, (c) specific heat, (d) mass fraction.

vortex shrinks and disappears completely as the freezing process completes [24].

3.3.2. Melting of composite phase change material

According to traditional methods, energy transportation over the fluid layers is only by conduction mode. However, the recent analysis proved that in the melting region natural convection also influences and plays a crucial role in heat transfer processes and it is observed that convection predominates in the melting phase. Visualization of patterns confirms that amid the melting process there is no variation in solid-liquid interface patterns. This demonstrates the natural convection of liquid CPCM and retains two-dimensional amid the entire melting process.

At this stage the viscous effect and gravity together overcome the buoyancy effect and causes no further movement of the melting front. The evolution of the melting front with time is as shown in Fig. 10. In the cooling process as heat extraction starts molten CPCM starts contracting and all particles come in contact with each other. This physical contact results domination of conduction and forms bulged shape.

3.3.3. Temperature distribution

The temperature contours of left wall heating are shown in Fig. 11. There are no significant changes in the temperature profiles with time, at adjacent to the hot wall some wavy shapes formed but the opposite side remained in the sub-cooled state. These wavy patterns indicate the uneven distribution of temperature over the surface of domain. Temperature magnitudes are maximum at the hot wall where molten CPCM is accumulated, temperature patterns at other parts are slightly uniform due to the solid phase of CPCM. When the heat extraction process starts molten CPCM begins to settle near the walls and results in the uniform temperature profile, as time progresses hot spot or molten CPCM starts squeezing toward the center.

3.4. Geometry orientation at 135°

3.4.1. Flow characteristic study

The melting process starts with predominant effect of conduction, due to the absence of natural convection and shows vertical interface patterns among liquid and solid phases. As time proceeds, the hot fluid ascents upwards and the cold liquid next to the solid succeeds. Hence, a recirculation vortex forms on the upper half of domain and natural convection plays a dominant role. But at the bottom, conduction remains predominant in half portion of domain. Over the longer duration further, natural convection turns out to be more significant and the

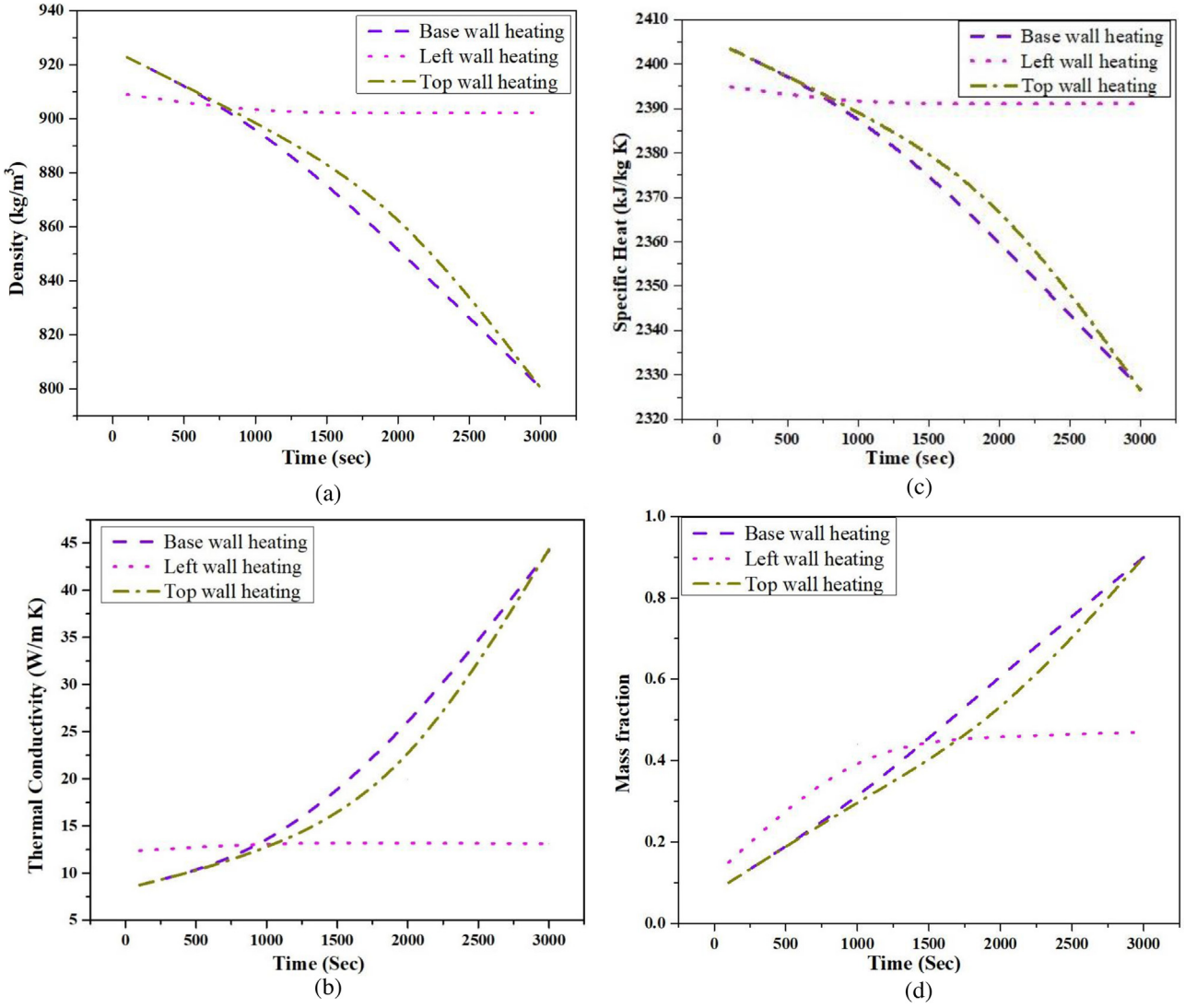

Fig. 16. Thermophysical properties variation in 90° orientation for different wall heating: (a) density, (b) thermal conductivity, (c) specific heat, (d) mass fraction.

melting rate gets faster on the upper half of domain. The CPCM changes its phases at this point and melting rate marginally reduced in the bottom portion of domain, as the reduction of heat conduction decreases due to the expansion of fluid layer thickness and thermal resistance. This is due to the presence of cool solid besides the left wall in the bottom portion of domain [25], the detailed patterns are shown in Fig. 12.

It is seen that, the solid-liquid interface patterns are irregular. The anisotropy of thermal conductivity and the crystallographic effects plays a dominant role in controlling the interface patterns. Completely molten CPCM forms circular vortex patterns when heat is extracted, as process continuous and at the completion of the solidification process the streamlines distribute uniformly all over domain.

3.4.2. Melting of composite phase change material

The majority of work done so far including numerical and experimental, a square/bounded domain with one wall heated condition considered to study the effect of natural convection above the melting temperature of the PCMs. The hydrodynamic and thermal layers formed in the melting region are 2-D under defined condition.

The highest temperature is at the hot wall and the CPCM starts melting from the hot wall since natural convection zone forms and further melts to result in the expansion of CPCM in domain. The detailed contours are as shown in Fig. 13. The left wall heating is an efficient way to achieve faster melting, at the intermediate stage only a small portion of the CPCM melted and the majority of domain is covered with partially molten mushy zone. The mushy region of CPCM stores relatively lower amount of heat compared to completely molten phase, the solidification process starts rapidly and freezing occurs in a much quicker way as the amount of heat stored is relatively small.

3.4.3. Temperature distribution

For the Left wall heating the temperature distribution is completely single sided, the profile shows hotspot only along the left vertical wall where heat flux is applied.

The temperature profile mimics the hot wall and patterns spreads uniformly over domain, detailed temperature distribution contour shown in Fig. 14. The steady temperature profiles, amid the early time of melting process temperature patterns are almost parallel to the hot wall showing that heat is transferred in the perpendicular direction to the heated wall and conduction is dominated. There is no change in the temperature profile at the sub-cooled regions near the isothermal wall. During the cooling process, the temperature patterns are somewhat disturbed in nature and form circular profiles all around molten CPCM.

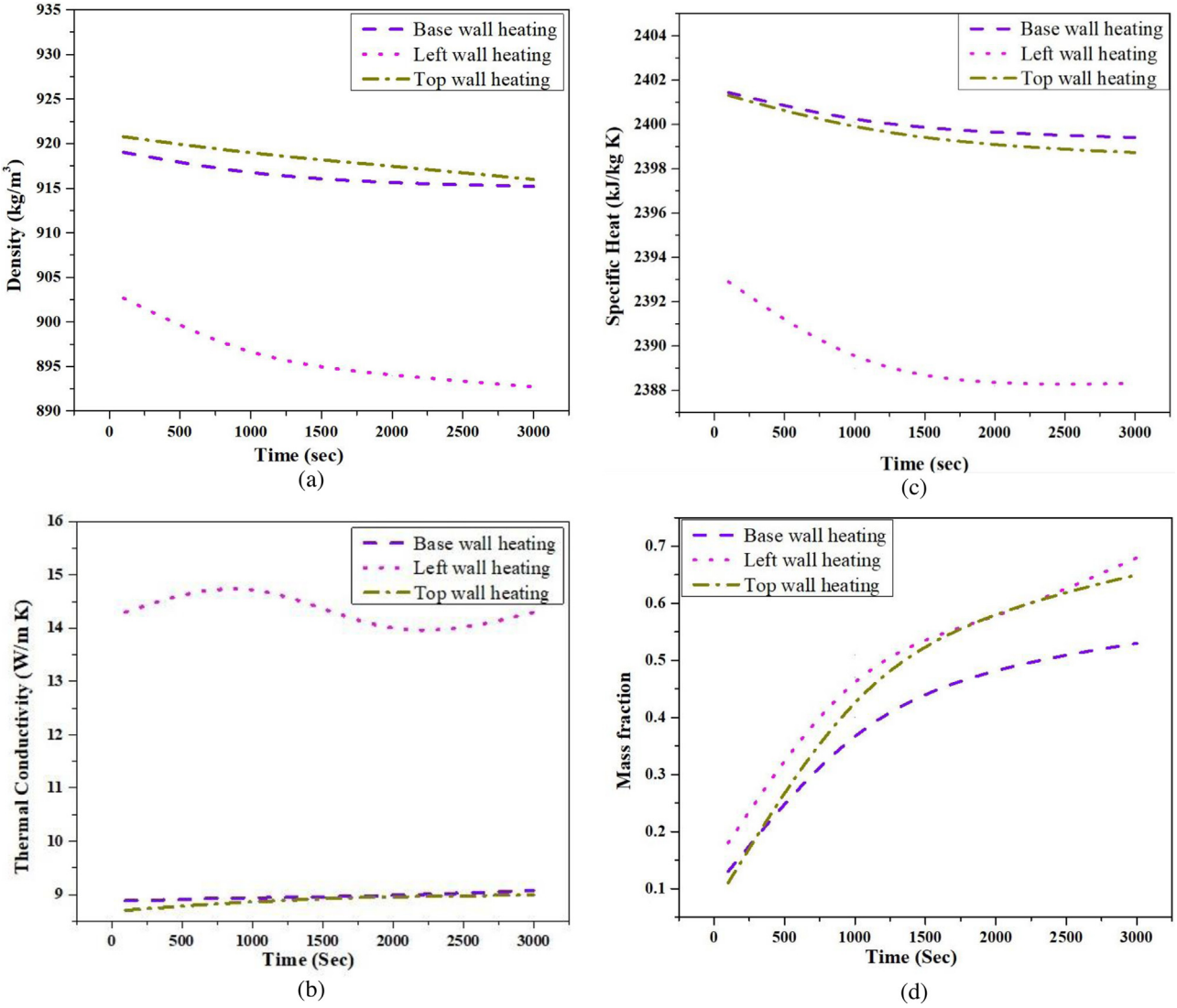

Fig. 17. Thermophysical variation in 135° orientation for different wall heating: (a) density, (b) thermal conductivity, (c) specific heat, (d) mass fraction.

3.5. Effect of orientation and different wall heating on mass fraction during melting and solidification process

Comparative study of the four cases leads to exciting results with different orientations and different wall heating's are discussed in the subsequent sections. Results of the three cases are summarized and it is understood that, only top wall heating provides faster and maximum melting fraction. The melting rate is much superior to the base and left wall heating cases. Left wall and base wall reached the average mass fraction only 0.47 and 0.69 respectively but top heating provided maximum value of average mass fraction 0.9 under the same operating conditions. For cooling cycle both left and base walls showed same response but top wall cooling rate is much higher. This faster solidification is may be due to the formation of a solid layer which provides larger area of exposure to solid CPCM and makes conduction dominated hence it promotes the heat transfer mechanism.

Base and left wall heating case results are identical for all the orientations and average mass fraction obtained over time period of 3000 s are 0.52 and 0.9 respectively. For top wall heating, results are entirely different, the average mass fraction is 1.0 which means the CPCM is completely melted. The reason behind is that more area of exposure available and domination of conduction. For shallow domain solidification mechanism top wall cooling exhibited excellent characteristics but for lower cooling rates base wall or left wall can be preferred though both cases give similar results.

3.6. Effect of orientation and different wall heating on thermophysical properties during melting and solidification process

3.6.1. Thermophysical properties variation for 45° orientation

Fig. 15(a) shows the density variation for different wall heating. Variation of thermophysical properties are studied and discussed, the density variation for all three-wall hating is observed and the maximum difference in density is seen for base wall heating than the other two cases. The thermal conductivity variation for 45° orientation is shown in Fig. 15(b). It is observed that for left wall heating initially it increased but at later stage top wall heating overtakes and shows maximum value for the same operating conditions.

Fig. 15(c) shows the specific heat variations for different wall heating. Base wall heating seems to be insignificant for this case. The variation of specific heat has inverse effect on the thermal conductivity because of increased thermal conductivity reduces the specific heat and the transfer of heat within the CPCM increases. When compared to the other two cases better storability can be achieved through base wall heating.

Fig. 15(d) shows the mass fraction variation for different wall heating. The mass fraction variation at initial time steps are almost linear for all cases, but as time proceeds to 2000 s, left wall heating

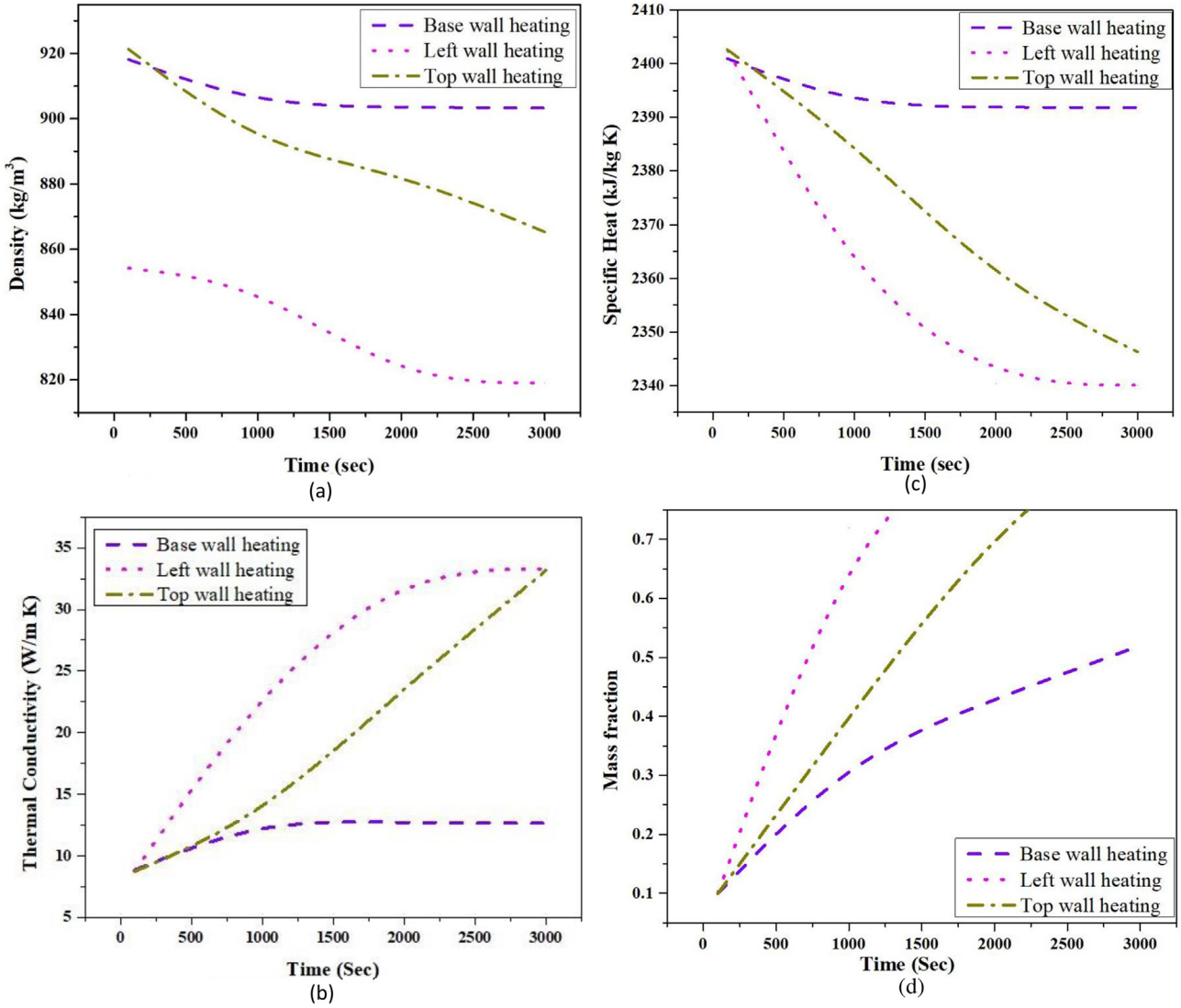

Fig. 18. Thermophysical variation in 180° orientation for different wall heating: (a) density, (b) thermal conductivity, (c) specific heat, (d) mass fraction.

shows faster melting rate. The area of melt front generated by molten CPCM is relatively more in this case. Even though the same amount of heat is supplied the melting rate is comparatively slow due to lack of contact between the melt front and the sub-cooled fluid.

3.6.2. *Thermophysical properties variation for 90° orientation*

When the orientation is changed to 90° which is referred to a deep domain. Fig. 16(a) shows the density variations for different wall heating. The different wall heating shown different responses by changing the thermophysical properties of CPCM enclosed in it. Left wall heating shown almost no change in the density as the melting fraction change is parallel to the hot wall and the change in density is negligible. For base and top wall heating density gets reduced as the mass fraction is higher and molten CPCM occupied more space compared to left wall heating. The mass fraction variation for base and top wall heating is almost the same due to area available for the interaction of heat is same. Thermophysical properties changed only during base and top wall heating, thermal conductivity increased almost linearly for both the cases and specific heat linearly gets reduced and it can be seen from Fig. 16(b).

In top and base wall heating cases, almost same amount of heat is absorbed by the material but in left wall heating initially mass fraction increased but it has reached maximum of 0.5 (shows only 50% melting). Mass fraction depends on the most of thermophysical properties, left wall heating provided almost no change in thermal conductivity and specific heat the variation can be seen from Fig. 16(c). These results indicate that thermal conductivity and specific heat capacity are inversely proportional properties the variation of the mass fraction for different wall heating can be understood from Fig. 16(d).

3.6.3. *Thermophysical properties variation for 135° orientation*

Fig. 17 shows the thermophysical properties variation for different wall heating cases. For 135° orientation for all the thermophysical properties variation are similar for the base and top wall heating but for left wall heating is slightly higher in variations. Density change is almost same for top and base wall but it is greatly reduced for left wall heating because the hot wall surface is higher and the material which is coming in contact also more and gets melted and density gets reduced. Mass fraction change for left wall is highest among all the cases because molten layer covers the top surface of solid material Fig. 17 (b) shows the thermal conductivity variations for different wall heating.

The gravity effect causes molten layer to flow downwards and the melting process gets accelerated, as molten material gets increased the thermal conductivity gets increased due to the presence of more conductive material. As already discussed, thermal conductivity has an adverse effect on specific heat. It gets reduced considerably for left wall heating. When thermal conductivity increases the heat carrying particles gets activated and material releases the heat quickly and hence the

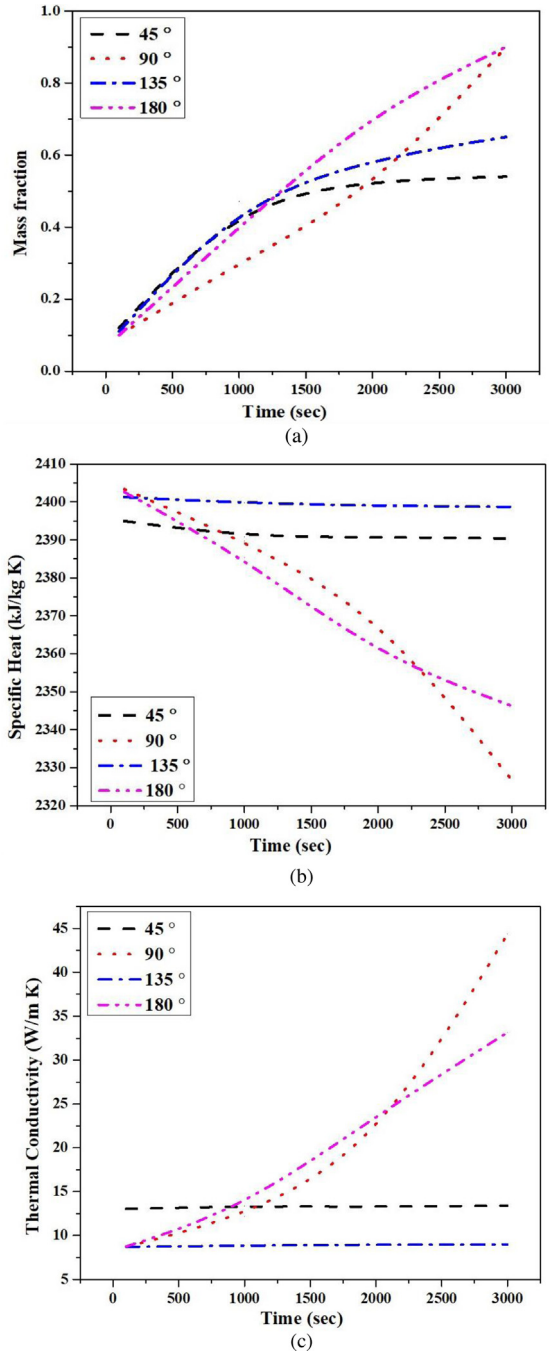

Fig. 19. Comparison of melting characteristics for top wall heating: (a) mass fraction variation, (b) specific heat, and (c) thermal conductivity variation with different orientations.

specific heat capacity gets reduced, Fig. 17(c and d) shows the specific heat and mass fraction variations for different wall heating.

3.6.4. Thermophysical properties variation for 180° orientation

Similar to the 135° orientation 180° also shows identical characteristics because of the same reason, the heat interaction area is more so the formation of molten layer is also high. Increase in melt fraction leads a reduction in density are more for left wall and approximately similar for the base and top wall. Mass fraction developed is obviously more for the left wall heating and it is similar to right wall heating. Top and base wall shown completely identical results, for this reason right wall heating is considered, Fig. 18(a and b) shows the density and thermal conductivity variations for different wall heating.

For thermal conductivity variation, it is observed that left and right wall heating caused almost the same effect on domain, the highest value for thermal conductivity is same. As thermal conductivity increased the CPCM releases the stored heat easily and leads faster discharging of heat. Compare to the left, base, and right wall heating is shown moderate values for the melting and heat-releasing duration by storing heat for the longer period of time, Fig. 18(c and d) shows the specific heat and mass fraction variations for different wall heating.

3.6.5. Comparison of top wall heating characteristics for different orientations

Overall analysis shows that the top wall heating exhibits comparatively better results, as compared to other wall heating. Top wall heating for all the orientations are further analyzed. The mass fraction variation in deep (90°) and shallow (180°) domains are much superior and reaches maximum (0.9) value at 2000 s. The mass fraction for 45° and 135° orientation s are not shown any significant change and maximum value reached only up to 0.65 even after 3000 s of heating time. The variation of mass fraction with different orientation is shown in Fig. 19(a).

The variation in specific heat for 45° and 135° are almost constant for all cases of heating time. The variation in deep and shallow domain shows a significant change and decreases with heating time. The specific heat value is drastically reduced for deep domain and reached to least value at 3000 s. The increase in liquid phase thermal conductivity is due to the increase in mass fraction. For deep (90°) domain the increase in mass fraction up to heating time 1500 s is linear (0.1–0.4) and corresponding thermal conductivity also linearly increased (7–15 W/m K). Whereas after 1500–3000 s mass fractions increased drastically (0.4–1.0) and thermal conductivity also followed the same trend (15–45 W/m K). Specific heat variation with different orientations is shown in Fig. 19(b).

As discussed earlier thermal conductivity and specific heat are inversely proportional properties, for deep and shallow domains thermal conductivity is maximum and reached up to 45 and 35 W/m K for deep and shallow respectively. After 3000 s of heating time for 45° and 135° orientations variation of thermal conductivity is negligible and remained constant throughout the melting process. However, for 45° orientation it is higher than 135° orientation variation of thermal conductivity variation for different orientations is shown in Fig. 19(c). The complete summary of all the cases are listed in Table 3 which shows comparative results of melting/solidification characteristics of CPCM for different orientations and wall heating cases.

4. Conclusions

Numerical study of the bounded domain with different orientations are analyzed through flow patterns and heat transfer parameters such as, thermal conductivity, specific heat, melting/solidification fractions for different time intervals. Three different heating cases (base, left and top wall) are studied for different geometrical orientations such as, 45°, 90° (deep), 135° and 180° (shallow) domains. An attempt has been made to understand the melting/solidification behavior for different heating walls. The heat transfer in the solidification process is by conduction but in the melting process it is by natural convection. It is seen that the following factors such as geometrical orientation, the direction of heating, gravitational effect, Buoyancy and viscosity greatly affected on the melting/solidification characteristics of the CPCM. Among three heating cases, top wall heating shows complete melting at a minimum time interval of 3000 s. This is because of faster melting rate raises molten material temperature and reduced viscosity leads to faster particle migration. Base and side wall heating shows relatively lower melting rate due to a larger sub-cooled region (for left and right) where the heat is not penetrated and the buoyancy effect is also very less. It can be concluded that for faster melting shallow domain with top wall heating can be preferred. Three-dimensional flow patterns and heat

Table 3
Comparison of melting/solidification characteristics of composite phase change material for different orientation and wall heating cases.

Parameters	Time (s)	45° orientation			90° orientation			135° orientation			180° orientation		
		Base wall heating	Left wall heating	Top wall heating	Base wall heating	Left wall heating	Top wall heating	Base wall heating	Left wall heating	Top wall heating	Base wall heating	Left wall heating	Top wall heating
Average density (kg/m^3)	500	912.43	904.71	909.61	922.78	909.00	922.78	919.02	902.67	920.78	918.18	854.23	921.34
	1000	903.53	901.46	902.00	899.09	902.27	899.08	916.46	895.71	918.86	904.18	849.38	891.47
	2000	902.74	899.52	901.60	852.37	902.12	868.74	915.55	894.00	917.48	903.51	819.30	883.38
	3000	904.87	896.71	901.05	800.50	902.28	800.32	915.20	892.72	915.98	903.29	819.05	865.30
Average thermal conductivity (w/m K)	500	11.81	12.54	13.03	8.73	12.37	8.73	8.88	14.30	8.70	8.85	8.75	8.75
	1000	12.51	12.76	13.36	12.15	13.22	12.15	8.94	15.08	8.88	12.96	23.66	13.19
	2000	12.63	13.44	13.26	25.01	13.18	19.95	8.97	13.66	8.96	12.69	33.15	23.66
	3000	12.97	13.81	13.43	44.24	13.12	44.35	9.08	14.30	8.99	12.65	33.27	33.15
Average specific heat (kJ/kg K)	500	2396.96	2392.58	2395.00	2403.42	2394.89	2403.42	2401.44	2392.9	2401.31	2400.98	2402.66	2402.66
	1000	2391.98	2390.80	2390.91	2389.68	2391.09	2389.68	2400.09	2389.00	2399.76	2392.18	2359.36	2385.28
	2000	2391.53	2389.55	2390.74	2360.55	2391.03	2370.92	2399.60	2388.21	2399.02	2391.91	2340.24	2359.36
	3000	2393.88	2387.95	2390.39	2326.79	2391.13	2326.66	2399.41	2388.32	2398.73	2391.81	2340.07	2346.24
Average mass fraction	500	0.16	0.21	0.12	0.10	0.15	0.10	0.13	0.18	0.11	0.10	0.10	0.10
	1000	0.40	0.48	0.47	0.30	0.44	0.30	0.40	0.51	0.47	0.33	0.72	0.40
	2000	0.45	0.50	0.53	0.61	0.46	0.50	0.49	0.57	0.59	0.43	0.90	0.72
	3000	0.45	0.69	0.54	0.90	0.47	0.90	0.53	0.68	0.65	0.52	0.90	0.90

transfer parameters will be the future work of the present study.

References

[1] D. Cano, C. Funéz, L. Rodriguez, J.L. Valverde, L. Sanchez-Silva, Experimental investigation of a thermal storage system using phase change materials, Appl. Therm. Eng. 107 (2016) 264–270.

[2] A. Barba, M. Spiga, Discharge mode for encapsulated PCMs in storage tanks, Sol. Energy 74 (2003) 141–148.

[3] N.S. Dhaidan, J.M. Khodadadi, T.A. Al-Hattab, S.M. Al-Mashat, Experimental and numerical investigation of melting of phase change material/nanoparticle suspensions in a square container subjected to a constant heat flux, Int. J. Heat Mass Transfer 66 (2013) 672–683.

[4] S.Z. Shuja, B.S. Yilbas, M.M. Shaukat, Melting enhancement of a phase change material with presence of a metallic mesh, Appl. Therm. Eng. 79 (2015) 163–173.

[5] B.W. Webb, R. Viskanta, Natural-convection-dominated melting heat transfer in an inclined rectangular enclosure, Int. J. Heat Mass Transfer 29 (1986) 183–192.

[6] H. Zennouhi, Effect of inclination angle on the melting process of phase change material, Case Stud. Therm. Eng. 9 (2017) 47–54.

[7] F. Al-Attar, M. Alsamhan, A. Al-Banna, J. Samuel, Thermal, Mechanical and rheological properties of low density/linear low-density polyethylene blend for packing application, J. Mater. Sci. Chem. Eng. 6 (2018) 32–38.

[8] C. Santosh, G. Veershetty, D. Arumuga Perumal, Preparation and characterization of nanoparticle blended polymers for thermal energy storage applications, AIP Conf. Proc. 2057 (1–8) (2019) 020028.

[9] A. Trigui, M. Karkri, I. Krupa, Thermal conductivity and latent heat thermal energy storage properties of LDPE/wax as a shape-stabilized composite phase change material, Energy Convers. Manage. 77 (2014) 586–596.

[10] C.S. Reddy, C.K. Das, Thermal and dynamic mechanical properties of low-density polyethylene-silica nano-composites: effect of zinc-ion coating on nanosilica, Polym. Polym. Compos. 14 (2006) 281–290.

[11] P. Sobolciak, M. Karkri, M.A. Al-Maadeed, I. Krupa, Thermal characterization of phase change materials based on linear low-density polyethylene, paraffin wax and expanded graphite, Renew. Energy 88 (2016) 372–382.

[12] T. Märtson, V. Krumme Gavrilkina, Viikna, The effect of modality on linear low-density polyethylene crystallization behaviour at high and very high supercoolings, Proc. Est. Acad. Sci. 58 (2009) 53.

[13] Na Li, H. Xuankai, Z. Haiyan, S. Zhicong, L. Yunyong, W. Chengxin, NaCl multistage-recrystallization-induced formation of 3D micro-structured ribbon-like graphene based films for high performance flexible/transparent supercapacitors, J. Mater. Chem. A 5 (2017) 14595–14603.

[14] C. Santosh, G. Veershetty, D. Arumuga Perumal, A review on thermal energy storage using composite phase change materials, Rec. Pat. Mech. Eng. 11 (4) (2018) 298–310.

[15] H. Mehling, C. Barreneche, A. Solé, L.F. Cabeza, The connection between the heat storage capability of PCM as a material property and their performance in real scale applications, J. Energy Storage 13 (2017) 35–39.

[16] Y. Xu, Y.L. He, G.H. Zhu, S. Lv, B. Shan, Al/Al_2O_3 form-stable phase change material for high temperature thermal energy storage, Energy Procedia 105 (2017) 4328–4333.

[17] V. Kapsalis, D. Karamanis, Solar thermal energy storage and heat pumps with phase change materials, Appl. Therm. Eng. 99 (2016) 1212–1224.

[18] X. Huang, G. Alva, L. Liu, G. Fang, Microstructure and thermal properties of cetyl alcohol/high density polyethylene composite phase change materials with carbon fiber as shape-stabilized thermal storage materials, Appl. Energy 200 (2017) 19–27.

[19] A.V. Arasu, A.S. Mujumdar, O. Al, O. Al, Numerical study on melting of paraffin wax with Al_2O_3 in a square enclosure, Int. Commun. Heat Mass Transf. 39 (2012) 8–16.

[20] M.J. Allen, N. Sharifi, A. Faghri, T.L. Bergman, Effect of inclination angle during melting and solidification of a phase change material using a combined heat pipe-metal foam or foil configuration, Int. J. Heat Mass Transfer vol. 80, (2015) 767–780.

[21] C. Santosh, D. Arumuga Perumal, G. Veershetty, Numerical studies for charging and discharging characteristics of composite phase change material in deep and shallow rectangular enclosure, IOP Conf. Ser. Mater. Sci. Eng. 376 (2018) 012059.

[22] M. Koller, H. Walter, M. Hameter, Transient numerical simulation of the melting and solidification behavior of $NaNO_3$ using a wire matrix for enhancing the heat transfer, Energies 9 (2016) 205.

[23] B. Kamkari, H. Shokouhmand, F. Bruno, Experimental investigation of the effect of inclination angle on convection-driven melting of phase change material in a rectangular enclosure, Int. J. Heat Mass Transfer 72 (2014) 186–200.

[24] V.R. Voller, C.A. Prakash, Fixed grid numerical modeling methodology for convection-diffusion mushy region phase-change problems, Int. J. Heat Mass Transfer 30 (1987) 1709–1719.

[25] M. Jourabian, M. Farhadi, A.A.R. Darzi, Simulation of natural convection melting in an inclined cavity using lattice Boltzmann method, Sci. Iran. 19 (2012) 1066–1073.